TITLE: Single-cell tracing dissects regulation of maintenance and inheritance of transcriptional reinduction memory

AUTHORS: Poonam Bheda[1], Diana Aguilar-Gómez[1-3], Nils B. Becker[4†], Johannes Becker[5†], Emmanouil Stravrou[6], Igor Kukhtevich[1], Thomas Höfer[4], Sebastian Maerkl[5], Gilles Charvin[7], Carsten Marr[8], Antonis Kirmizis[6*] and Robert Schneider[1,9*]

AFFILIATIONS:

[1] Institute of Functional Epigenetics, Helmholtz Zentrum München, Neuherberg, Germany.

[2] Center for Genomic Sciences, UNAM, Cuernavaca, Mexico.

[3] Center for Computational Biology, UC Berkeley, Berkeley, USA.

[4] Theoretical Systems Biology, DKFZ, Heidelberg, Germany.

[5] Institute of Bioengineering, School of Engineering, École Polytechnique Fédérale de Lausanne, Lausanne, Switzerland.

[6] Biological Sciences, University of Cyprus, Nicosia, Cyprus.

[7] Development and Stem Cells, IGBMC, Strasbourg, France.

[8] Institute of Computational Biology, Helmholtz Zentrum München, Neuherberg, Germany.

[9] Lead author

†indicates equal contribution

*Corresponding authors: robert.schneider@helmholtz-muenchen.de, kirmizis.antonis@ucy.ac.cy

SUMMARY

Transcriptional memory of gene expression enables adaptation to repeated stimuli across many organisms. However, the regulation and heritability of transcriptional memory in single cells and through divisions remains poorly understood. Here, we combined microfluidics with single-cell live-imaging to monitor *Saccharomyces cerevisiae* galactokinase 1 (GAL1) expression over multiple generations. By applying pedigree analysis we dissected and quantified maintenance and inheritance of transcriptional reinduction memory in individual cells through multiple divisions. We systematically screened for loss- and gain-of-memory knockouts to identify memory regulators in thousands of single cells. We identified new loss-of-memory mutants, which strikingly affect memory inheritance into progeny. Importantly, we also unveiled a novel gain-of-memory mutant, *elp6Δ*, and demonstrated that this new phenotype can be mediated through decreased histone occupancy at the GAL1 promoter. Our work uncovers principles of maintenance and inheritance of gene expression states and their regulators at the single-cell level.

INTRODUCTION

When certain genes are repeatedly exposed to the same stimulus they can adapt subsequent responses. This so-called transcriptional reinduction memory is important for adaptation of gene expression across various organisms. Emerging evidence suggests that transcriptional memory could have important consequences on cell survival and identity (Foster et al., 2007; Francis and Kingston, 2001), and that it could have implications for disease progression e.g. in diabetes (Villeneuve et al., 2011) and innate immunity in humans (Foster et al., 2007). Thus, a comprehensive understanding of transcriptional memory has become increasingly important.

Although an epigenetic basis for some reinduction memory systems has been suggested (Avramova, 2015; Berry et al., 2017; D'Urso and Brickner, 2017; Iberg-Badeaux et al., 2017), there has been a lack of approaches and measures to quantify the maintenance and inheritance of memory through cell divisions mainly due to the use of bulk cell populations which masks single-cell behavior. To address the potential epigenetic nature of such a transcriptional memory, tracking of single cells over multiple cellular generations through cell divisions is necessary. Here we establish a novel combination of single-cell approaches to trace and quantify the maintenance and inheritance of transcriptional memory in individual cells through repeated stimuli and identify novel regulators of memory. We chose *S. cerevisiae* Gal1 (Galactokinase 1) as a model gene first because of its previously characterized reinduction memory (Kundu et al., 2007; Kundu and Peterson, 2009, 2010; Sood and Brickner, 2017; Sood et al., 2017; Stockwell and Rifkin, 2017; Zacharioudakis et al., 2007), where more Gal1 is expressed in a repeated induction with galactose than in naïve cells partly due to changes in chromatin architecture (Kundu and Peterson, 2009; Sood et al.,

2017), and second because asymmetric budding facilitates cell- and lineage-tracking. Whereas factors regulating Gal1 induction such as Gal4, Gal80, and RSC are well described (Floer et al., 2010; Lohr et al., 1995), the reinduction memory is far less understood. Additionally, most studies of Gal1 reinduction memory have so far focused on cell populations and the inheritance of this memory within single-cell lineages has not been characterized.

Our microfluidic techniques for single-cell capture and observation over time combined with novel analyses allowed us to quantitatively investigate memory of gene expression in individual cells through divisions (maintenance) as well as transmission from a mother cell to its daughters (inheritance). Applying this we (i) identified not only deletions that negatively affect transcriptional memory but also a new gain-of-memory phenotype and (ii) dissected their effects on reinduction memory maintenance and inheritance.

RESULTS

Gal1 transcriptional memory is maintained through repression in individual mother cells

To characterize maintenance and inheritance of Gal1 transcriptional reinduction memory in single wild-type (WT) *S. cerevisiae* cells, we used time-lapse microscopy coupled to a microfluidics device to observe expression of a Gal1-GFP fusion over time in individually tracked cells (Figure 1A and Tables S1-S2). This custom-made cell-tracking microfluidics device traps individual yeast cells and allows for automated media changes and imaging. Individual cells can be monitored and fluorescence intensities quantified over time through growth up to eight generations. Plotting single-cell traces of Gal1-GFP intensities of

yeast cells (and any of their arising progeny) subjected to repeated GAL1 repression in glucose (glu) and induction in galactose (gal) reveals higher Gal1-GFP intensity in individual cells in the second induction (i2) compared to the first (i1) (Figure 1B). We confirmed that this reinduction memory is also present on the transcriptional level since we observed higher Gal1 RNA levels in i2 by bulk RT-qPCR (Figure S1), in agreement with previous findings in different strain backgrounds (BY4741-based and W303-based) (Brickner et al., 2007; Halley et al., 2010). We then compared Gal1 expression in individual mother cells (M, defined here as cells present in both i1 and i2) over time and observed that reinduction memory is higher at all comparable timepoints within each individual cell throughout all of i2 (Figure 1C). This demonstrates that transcriptional memory is maintained through repression in individual mother cells.

For quantitative comparisons of i1 versus i2, we dissected Gal1 expression kinetics into fluorescence intensity and delay (time from galactose exposure to detectable Gal1-GPF signal). Since we observed memory from start to end of induction (Figure 1C), we compared fluorescent intensities at just a single timepoint at the end of each induction. We found that >93% of mother cells maintain Gal1 reinduction memory according to either measure (Figure 1D, left and middle). While there is a significant difference in delay between i1 and i2 (Figure 1D, middle), expression rates are similar (Figure 1D, right. For statistical tests and *P*-values see Table S3). This reveals that reinduction memory maintenance in mothers leads to higher gene expression in i2 mainly due to shorter delay.

Gal1 transcriptional reinduction memory is inherited by naïve daughter cells

Our microfluidics setup allows us to define pedigrees using lineage-tracking based on asymmetric budding of mother cells. By establishing pedigrees we can distinguish

maintenance in mother cells (M) from the inheritance of reinduction memory into their galactose-naïve progeny (daughters, D, defined here as cells born during r2, Figure 2A), which is not possible from bulk population measurements. Strikingly, naïve daughters behaved like their pre-exposed mothers both in terms of intensity (Figure 2A) and delay (Figure 2B), demonstrating inheritance of transcriptional memory. Importantly, we then quantified memory inheritance from mothers to daughters by comparing their pairwise expression trajectories. To remove the general trend of cells being induced and expressing Gal1, which results in extremely high correlations even in unrelated cells due to the general induction trend, we calculated partial correlations (PCs) using average Gal1 expression in the population at each timepoint as the controlling variable. PCs between mother-daughter intensities over time during i2 revealed a 63% median PC between related pairs (M2-D2) compared to no correlation (0%) for random pairs (U M2-D2, Figure 2C). This demonstrates that the capacity for reinduction memory is inherited through cell division and provides novel quantitative measures for memory inheritance applicable to compare memory effects. Overall, our single-cell analysis shows that reinduction memory is established and maintained in mother cells, and efficiently transmitted through repression (r2) to their progeny.

The mechanisms underlying Gal1 reinduction memory are unclear and somewhat controversial. Previously, protein carryover from an initial induction has been shown to contribute to Gal1 reinduction memory (Kundu and Peterson, 2010; Zacharioudakis et al., 2007). When galactose is available, Gal3 binds and removes the Gal80 repressor from the Gal1 promoter, allowing the GAL genes to be expressed (Lohr et al., 1995). As Gal1 is a paralog of Gal3, it also has the ability to remove the Gal80 repressor; therefore, during reinduction undegraded Gal1 could contribute to memory. Chromatin structure has also been

implicated in reinduction memory especially during shorter repression intervals (Kundu et al., 2007; Kundu and Peterson, 2009; Sood and Brickner, 2017; Sood et al., 2017; Stockwell and Rifkin, 2017). Chromatin remodeling by Swi2 is involved in Gal1 induction, and deletion of Swi2 results in a decrease in memory (Kundu et al., 2007). On the other hand, it has been suggested that deletion of the histone H3K4 trimethyltransferase Set1 could enhance reinduction (Zhou and Zhou, 2011).

We were interested in determining the role of these factors in our media change protocol and microfluidics setup. We replaced the Gal1 ORF with GFP and tagged Gal3 with a C-terminal mCherry in order to observe their expression during a microfluidic memory experiment. Our results show that cells that reinduce GFP the highest from the Gal1 promoter are not the ones with the highest Gal3 levels prior to reinduction (Figure S2A). Given that Gal1 is deleted in these cells, and high Gal3 protein levels are not correlated with increased memory, we next investigated whether any protein expression during i1 is essential for reinduction memory. To address this, cells were induced with galactose while simultaneously inhibiting protein translation with cycloheximide (CHX) during i1 such that Gal1 mRNA could be transcribed without translation of the Gal1 protein (and any other nascent protein). In CHX-treated, galactose-induced cells, we observed Gal1 mRNA expression but no detectable Gal1-GFP protein during i1, and still witnessed reinduction memory in these cells in i2 (Figures 2D, S2B – C). Finally, we addressed whether reinduction memory transmittance from mother to daughter and hence the number of cell divisions during repression “dilutes” mother memory. Intriguingly, mother cells maintain their gene expression memory independently of the number of progeny produced, signifying that dilution of i1-expressed proteins does not influence i2 induction intensities and therefore memory (Figure 2E).

These results and other recent findings (Cerulus et al., 2018; Sood and Brickner, 2017; Sood et al., 2017) suggest that, besides the established *trans*-acting proteins (Zacharioudakis et al., 2007), chromatin components could be implicated in Gal1 transcriptional memory in our setup. Indeed, deletion of Swi2 in our Gal1-GFP reporter strain resulted in a decrease in memory, recapitulating previous findings on the role of this chromatin remodeler in Gal1 memory (Figure S2D, left). Incidentally, deletion of Set1 resulted not only in high expression during reinduction, as reported previously (Zhou and Zhou, 2011), but also during the initial induction. This indicates a general effect of *set1Δ* on Gal1 expression and therefore not a memory-specific phenotype (Figure S2D, right). This could be due to differences in the media changes that affect the extent of Gal1 repression (Stockwell et al., 2015) or because previous studies analyzed shorter timescales (Zhou and Zhou, 2011). Altogether, the above work prompted us to systematically screen for chromatin factors that can affect maintenance and/or inheritance of memory, resulting in an overall loss- or gain-of-reinduction memory in our microfluidics setup in comparison to WT.

Deletion of Cit1 and Set3 cause loss-of-memory, while Elp6 deletion results in a gain-of-memory phenotype

To identify novel chromatin-related loss- and gain-of-memory effectors in an unbiased approach we screened a library of 567 knock-out strains harboring the Gal1-GFP reporter and a single gene knockout (Figure 3A, Table S4) focused on non-essential chromatin-related factors. This library was produced by SGA (synthetic genetic array), a method for semi-automated large-scale genetic manipulation. SGA involves mating the haploid Gal1-GFP reporter strain with a library of deletions in the opposite mating type background to produce diploids, followed by sporulation and selection of haploids containing both the reporter and a single gene deletion. We employed a high-throughput microfluidics

platform (Denervaud et al., 2013) with 1152 chambers for simultaneous screening of each mutant strain in duplicate (and multiple WT replicates) with automated media changes and a segmentation pipeline for single-cell analysis (Figure S3A-C).

Based on single-cell Gal1 expression profiles, we observed higher expression in i2 in the WT, validating the presence of transcriptional reinduction memory in this microfluidics setup (Figure 3B). With this high-resolution and high-throughput approach we systematically compared strains and identified outliers with altered behavior in expression (Figure 3C, left) and/or delay (Figure 3C, right). We hypothesized that deletion of some Gal1 transcriptional machinery components might affect Gal1 induction, and indeed found that inactivation of RSC (Floer et al., 2010)(data not shown) or the Gal4 transcriptional activator resulted in generally poor induction, not specific to reinduction. To identify outliers specifically during the second induction based on fluorescence intensity, we compared the average fluorescence for each strain in each induction against the average fluorescence of all other strains at that timepoint as a more robust measure than comparing to WT only (see Methods, Figure 3C, left). To identify outliers based on delay, we compared the delay for each strain until 50% of cells were expressing Gal1 in each induction (Figure 3C, right). By applying these measures we discovered multiple previously unknown loss-of-memory mutants but remarkably also novel gain-of-memory candidates. For 30 candidates we recreated knock-out strains by homologous recombination and performed independent single-cell tracking microfluidics experiments. This allowed us to validate *set3Δ* and *cit1Δ* as the most striking loss-of-memory mutants and *elp6Δ* as the most robust gain-of-memory (Figures 3D and S4A). We also confirmed these phenotypes at the transcript level (Figure S5). As shown by comparing mutant strains with WT at equivalent i1 induction levels (Figures 3D and S4A) or thresholding for the same i1 expression level in all strains (Figure S4B, middle panel), these

loss- or gain-of-memory phenotypes are not simply due to overall impaired or enhanced induction. In line with this, exclusion of 'non-inducers' (Figure S4C) within the loss-of-memory populations did not change their phenotypes (Figure S4B, bottom panel).

Our cell-tracing analysis allows us to quantify and study the variability in Gal1 expression dynamics and also to distinguish sublineages within the population. By calculating a coefficient of variation for all cells (related and unrelated) in the population, we detected a high population variation specifically in Gal1 reinduction in *set3Δ* and *cit1Δ*, but not WT and *elp6Δ* (Figure 3E, left panel). As increased variability is correlated with slower growth rates (Keren et al., 2015), we compared doubling times (Schmidt, 2018) for each strain and found that there are no significant differences between the mutants and WT except for *cit1Δ*, which actually seems to grow faster (*P*-value = 0.0133, Mann-Whitney U with Bonferroni correction). Therefore slower growth rates are not the underlying source of variability in the loss-of-memory mutants. Rather, by comparing coefficients of variation between groups of related cells within each strain (sublineages) we found that this variability is partially due to particular sublineages of non-inducers or very slow inducers in *set3Δ* and *cit1Δ* (Figure 3E, right panel). This observation points to an inheritable inducing state. While Set3, a member of a histone deacetylase complex, has previously been implicated in decreased Gal1 reinduction (Kim et al., 2012), Cit1 and Elp6 represent novel regulators of Gal1 memory. Cit1 is a factor utilizing mitochondrial acetyl-coA (Kim et al., 1986) and Elp6 is a subunit of the so-called 'Elongator' (Elp) complex (Krogan and Greenblatt, 2001). Thus, our screening identified new pathways modulating transcriptional reinduction memory and even an unanticipated gain-of-memory phenotype.

Deletion of Cit1 results in asymmetric memory inheritance

Next, applying the quantitative measures we developed for WT yeast (see above) we used our pedigree analysis to dissect how these mutations specifically affect reinduction memory maintenance and/or inheritance. We first focused on memory maintenance effects by examining the relative difference (RD) between delay in expression in i1 and i2 of the same mother cell (M1-M2), which was calculated by dividing the absolute value of the difference in delays by the sum of the delays. We observed that *elp6Δ* strains exhibits a higher RD in delay while *cit1Δ* has lower RD in comparison to WT (Figure 4A). This demonstrates that effects on transcriptional reinduction memory maintenance in mothers contribute to both gain-of-memory and loss-of-memory phenotypes. In general *set3Δ* and *cit1Δ* mother cells have longer delays than WT, while in *elp6Δ*, we observed no effects on i1 delay, but significantly shorter i2 delays than WT (Figure 4B). Due to positive feedback in the Gal network, the expression rate depends on the delay – cells that start expressing earlier have a higher expression rate in comparison to cells that start expressing later. To eliminate differences due to the delay, we compared expression rates of mothers with similar delays and observed no effects on the expression rate in *set3Δ* and *cit1Δ* in either i1 or i2 (Figure 4C). Comparison of *elp6Δ* mothers with similar delays as WT, however, reveals similar expression rates in i1 but an increased expression rate in i2 (Figure 4C). These data, corroborated by linear fits of M1-M2 intensity scatter plots (Figure S6), support a reinduction memory model where gain-of-memory affects both the delay and expression rate during memory maintenance in mothers, whereas loss-of-memory affects only delay in i2. This indicates that both types of mutants act through the maintenance of reinduction memory in the mothers.

To investigate specific effects on the inheritance of memory into daughters, we compared mothers with their respective daughters in i2 (M2-D2) again using partial

correlation (PC). This analysis revealed that *cit1Δ* has a significantly lower M2-D2 PC (Figure 4D), indicating that mothers and daughters do not follow the same trajectory of Gal1 expression. In addition, *cit1Δ* mothers and daughters have a high relative delay difference (RD, Figure 4E), i.e. Gal1 expression delays differ within each mother-daughter pair. While both the PC and RD can reveal differences between mothers and daughters, neither measure indicates whether there is indeed a defect in daughter memory inheritance; therefore we employed Bayesian statistics with posterior distribution functions to determine whether there is any bias in mothers or daughters expressing first. We found that *cit1Δ* is the only strain with a probability skewed towards mothers expressing Gal1 before their daughters in i2 (Figure 4F). This suggests that loss of Cit1, unlike our other loss-of-memory mutant *set3Δ*, results in a defect in memory inheritance. This unveils the first mutant with a described asymmetric transcriptional reinduction memory inheritance, exacerbating the loss-of-memory phenotype.

Gain-of-memory is a property of Elp complex members, resulting from incomplete nucleosome reincorporation during repression

We then focused on the intriguing gain-of-memory phenotype we discovered in *elp6Δ*. Elp6 is part of a 6-member Elongator complex of proteins (Krogan and Greenblatt, 2001). Independent deletions of 3 other non-essential Elp subunits also exhibited memory enhancement (Figures 5A and S7) demonstrating that this gain-of-memory phenotype is a property of a dysfunctional Elp complex. Our cell-tracking allowed us to further analyze the *elp6Δ* gain-of-memory phenotype according to expression levels in i1. We sorted cells into three i1 expression bins – low, medium, and high – and found that a stronger first induction leads to an even stronger *elp6Δ* gain-of-memory phenotype in comparison to WT (Figure S8). Further dissection of *elp6Δ* tracking and lineage revealed that *elp6Δ* has a discernible effect

on delay differences (RD) between mother and daughter cells in i2 (Figure 4E), but no effect on the mother-daughter induction dynamics (PC, Figure 4D) or bias towards mothers or daughters expressing first (Figure 4F). This lack of bias and no effect on PC indicate that the observed mother-daughter delay differences are not due to altered inheritance. Considering the previous known links of the Elp complex with chromatin and transcription (Li et al., 2009; Svejstrup, 2007) we hypothesized that its effects could stem from changes in promoter activation prior to Gal1 detection.

To explore how a chromatin-based gain of transcriptional reinduction memory could contribute to mother-daughter delay differences we devised a minimal model for Gal1 expression. We envisioned gene activation as a series of sequential activation steps (i1, Figure 5B), including chromatin-related processes such as nucleosome remodeling, histone modifications, and transcriptional machinery recruitment, leading to Gal1 promoter activation and expression. Soon after glucose-induced repression, preinitiation complex components and RNA polymerase II are not detected at the Gal1 promoter (Kundu et al., 2007) suggesting that cells cascade back to an inactive state (r2, Figure 5B), and that WT memory may be due increased activation rates in i2. We considered two gain-of-memory hypotheses (Figure 5C) where manipulation of chromatin-related processes could lead to shorter delays and hence the gain-of-memory phenotype that we observed in *elp6Δ* (Figure 4B, right panel): either the rates of the individual activation steps in i2 are even larger in *elp6Δ* than in WT, or *elp6Δ* requires less reactivation steps than WT (Figure 5C). We tested which of the two hypotheses is more likely with a quantitative stochastic model of stepwise activation. Our model consists of two parameters: the number of activation steps n and the activation rate α (see Methods for details). We found that a model where the number of activation steps is reduced in *elp6Δ* while the activation rate α is unchanged can explain both effects observed in the data: a

shorter delay in *elp6Δ* and a larger relative mother-daughter difference (Figure 5D). Mechanistically, gain-of-memory and faster reinduction based on a reduced number of steps of reinduction steps could be explained by *GAL1* being 'primed' for reactivation, for example by altered nucleosome occupancy. To test for this possibility we performed ChIP for histone H3 at *GAL1*. We found that H3 levels at *GAL1* at the end of r2 in *elp6Δ* remain significantly lower than in WT (Figure 5E). To further substantiate this finding, we compared nuclease sensitivity at the *GAL1* promoter in WT and *elp6Δ* at the end of r2 and found that *elp6Δ* chromatin can be more susceptible to nuclease digestion compared to WT (Figure 5F). Both the results from the H3 ChIP as well as the nuclease sensitivity assay strongly suggest that incomplete nucleosome reincorporation during repression, which in turn maintains an open-chromatin state that is permissive for faster Gal1 reinduction, contributes to the unexpected gain-of-memory phenotype. This implies a potential novel function for the Elp complex in facilitating nucleosome restoration during repression, in line with previous findings on Elp complex involvement in nucleosome assembly (Li et al., 2009).

DISCUSSION

Our combination of experimental single-cell approaches, pedigree analysis, and mathematical modeling allowed us to discover new loss-of-memory and gain-of-memory effectors. It also highlights the powerful nature of single-cell tracking approaches to tackle fundamental biological questions.

For the memory factors Elp6, Cit1 and Set3 we applied pedigree analysis to dissect their effects on maintenance of reinduction memory in mother cells through cell divisions and effects on inheritance into daughter cells. We found that these mutants can affect the kinetics

of the Gal1 promoter reaching its fully active (or repressed) state, and alter the timing of transcription during reinduction. We were surprised to identify a gain-of-memory mutant, and thus focused our further studies on this phenotype. The Elp complex was originally identified as playing a role in transcriptional elongation along with RNA polymerase II (Otero et al., 1999). However, it has since been implicated in various cellular processes, including tRNA modification as well as histone acetylation, nucleosome assembly and transcription (Chen et al., 2011; Esberg et al., 2006; Li et al., 2009; Rahl et al., 2005; Svejstrup, 2007) though its exact function is still unclear. This makes understanding its precise molecular role in Gal1 memory challenging. Interestingly, Elp components have been shown to be present at the *GAL1* locus (Santisteban et al., 2011). Since histone acetyltransferase activity through its Elp3 subunit has been described (Winkler et al., 2002; Wittschieben et al., 1999), it is possible that disruption of the complex and its histone-modifying activity could affect histone deposition at *GAL1*, leading to the faster reinduction that we observed. In line with this, incorporation of a partially unwound H2A.Z-containing nucleosome by the RSC complex at the Gal1 promoter facilitates Gal4 transcriptional activator binding, nucleosome loss, and faster induction (Floer et al., 2010).

We propose that Elongator may directly alter chromatin organization at *GAL1* by affecting nucleosome restoration during repression, thereby priming *GAL1* for reactivation (Figure 5F) and contributing to the gain-of-memory phenotype. This is supported by our ChIP and nuclease sensitivity data and mathematical modelling. A prediction from this would be that *elp* mutants might enable a cell to tolerate longer repression times, without losing transcriptional reinduction memory, and memory-storage capabilities at other inducible Elp complex targets in an *elpΔ* background. In higher eukaryotes, a combination of altered nucleosome occupancy (as observed in our yeast model) and/or the absence of repressive

histone modifications during repression could achieve a similar gain-of-memory phenotype.

While the mechanisms underlying transcriptional memory have been elusive, chromatin does seem to play a role. We observed memory independent of Gal1 and not correlated with Gal3 levels in our approach, and found that deletion of the chromatin remodeling factor Swi2 indeed results in reduced memory, pointing to a role for chromatin. The roles of various factors are, however, affected by the media change protocols, especially by the length of repression (Kundu and Peterson, 2010; Stockwell et al., 2015). For example, *set1Δ* did not show a memory-specific phenotype as was previously suggested, but rather an increase in Gal1 expression in both inductions in our media change protocol where we have the same length of glucose repression prior to each induction.

Our screening revealed that deletion of Set3 results in loss-of-memory, a phenotype that was also observed previously (Kim et al., 2012); however, *set3Δ* was only investigated in bulk populations and its effects on memory maintenance and inheritance were not studied. It is plausible to assume a role of its histone deacetylase activity in the loss-of-memory phenotype (Kim et al., 2012). Our screening also identified Cit1 as a novel regulator of Gal1 reinduction memory. Intriguingly, Cit1 protein levels have been shown to positively correlate with shorter delays during Gal1 reinduction (Cerulus et al., 2018). This is in line with our finding that Cit1 deletion results in longer delays during reinduction, which leads to its loss-of-memory phenotype. We found that Cit1 has a striking effect on memory inheritance and *cit1Δ* mother cells induce Gal1 before their daughters. Inheritance analyses, such as those described herein, require images with high temporal resolution as in our setup, which can affect the cellular well-being (e.g. growth rates). Therefore, it is vitally important to consistently compare experimental strains to a corresponding WT control, as we did in our studies. It is currently unclear why *cit1Δ*, unlike our other loss-of-memory mutant *set3Δ*,

results in such impaired transcriptional memory inheritance – perhaps the compromised metabolic state in *cit1Δ* (Cerulus et al., 2018) is better tolerated by mother cells.

Over all our inheritance analysis suggests that there are distinct mechanisms of establishment and inheritance of transcriptional reinduction memory in yeast cells. It supports a model where gain-of-memory affects both the delay and expression rate during memory maintenance in mothers, whereas loss-of-memory likely affects only delay in i2. We observed that inheritance can be asymmetric with an even stronger loss of memory in the daughters, as the case in *cit1Δ*, or can be a symmetric gain-of-memory with high variability as observed in the daughters of *elp6Δ* (Figure 6).

The memory mutants we identified function by affecting a combination of resources and chromatin-related processes involving nucleosomes and histone modifications directly or indirectly and provide us with novel effectors of Gal1 memory. This suggests that heritable chromatin states can indeed contribute to reinduction memory in addition to protein-based feedback loops (Kundu and Peterson, 2010; Stockwell and Rifkin, 2017; Zacharioudakis et al., 2007). The top 30 factors identified from our high-throughput screening can regulate a wide range of target genes beyond *Gal1*. This opens up the possibility that transcriptional memory occurs at many more genes that can be induced and also in other organisms where these factors are conserved. The existence of a gain-of-memory phenotype hints that there might be an optimal range of transcriptional memory. Whereas some memory can offer a competitive advantage in nutrient-limited environments, enhanced memory may result in a loss of bet-hedging strategies necessary to deal with repeated stresses.

It has become clear that studying whole populations of cells has so far limited our

understanding of transcription dynamics and in particular the inheritance of transcriptional states. Our approach relies on the implementation of microfluidic technologies for both high-throughput screening as well as in-depth lineage analyses on inheritance of transcriptional/chromatin states. More generally, the microfluidics technologies are not limited to studies of transcription, but will also be useful to studies of cell size, cell cycle, aging, and more. With rapidly developing microfluidics technologies as well as the discovery of feasible approaches to reporter and mutant library construction, we expect that our workflow can now be applied to various organisms, including mammalian cells, which will open up avenues to understand human cell behavior, in particular towards disease tolerance and cell heterogeneity.

ACKNOWLEDGEMENTS

We thank Youlian Goulev for support on the cell-tracking microfluidics setup and Michael Strasser for guidance on the modeling. We thank Matthias Meurer/Michael Knop and Ben Timney/Michael Rout for plasmids and Charlie Boone for yeast strains. Work in the R.S. laboratory was supported by the DFG through SFB 1064 and SFB 1309, the EpiTrio consortium as well as AmPro program (ZT0026) and the Helmholtz Gesellschaft. A European Research Council (ERC) starting grant, no. 260797, supported work in the A.K laboratory. P.B. is a Marie Curie IIF fellow and an EMBO LTF fellow. J.B. and S.J.M. were supported by a SystemsX.ch grant DynamiX-RTD (2008/005) and EPFL. G.C. was supported by a grant ANR-10-LABX-0030-INRT, a French State fund managed by the Agence Nationale de la Recherche under the frame program Investissements d'Avenir ANR-10-IDEX-0002-02.

AUTHOR CONTRIBUTIONS

P.B., A.K and R.S. conceived the study. E.S. and A.K. constructed the reporter library. J.B. performed the high-throughput microfluidic screen, and J.B. and S.J.M. designed the experiment, analyzed the data and identified memory mutant candidates. P.B., D.A.G., and I.K. performed the cell-tracking microfluidics time-lapse experiments and processed the data. G.C. developed the cell-tracking microfluidics and the cell-tracking image analysis pipeline. P.B., D.A.G., C.M. and N.B. analyzed the cell-tracking microfluidics data. D.A.G., P.B. and C.M. developed the model and performed the corresponding analysis. S.M., G.C., T.H., N.B. and C.M. critically revised the manuscript. P.B., A.K. and R.S. wrote the manuscript.

DECLARATION OF INTERESTS

Data and analysis scripts for cell-tracking microfluidics are available from the authors upon request. Code for stochastic delay model is available on Github (https://github.com/ccmarr/yeast-delay). Datasets generated from the high-throughput microfluidics screen are available upon request from Sebastian Maerkl.

The authors declare no competing financial interests. Correspondence and requests for materials should be addressed to robert.schneider@helmholtz-muenchen.de.

METHODS

Construction of the Gal1 reporter yeast strains. A precursor (RSY15) to the Gal1-GFP reporter strains RSY17 and RSY208 was constructed in parent strain Y7092 (SGA WT query strain, MATα *can1Δ*::STE2pr-Sp_his5 *lyp1Δ his3Δ1 leu2Δ0 ura3Δ0 met15Δ0*) as a C-

terminal fusion with GFP by transformation of a PCR product containing a superfolder GFP fused to a Cln2 PEST sequence with a kanMX cassette for selection using oligos OL2078 and OL2079 and plasmid pMaM4 as a template. The selection marker in this strain was changed to natMX (conferring resistance to cloNAT/Nourseothricin) to produce RSY17 (for selection during library construction) by PCR-mediated homologous recombination of natMX amplified by oligos OL2080 and OL2079 from plasmid p4339. For cell-tracking microfluidics experiments, RSY17 was also transformed with plasmid PL1603 containing an integrating nuclear marker consisting of an NLS-fused 2mCherry to create RSY208. For the RSY19 strain where Gal1 is replaced with GFP, and Gal3 is tagged with mCherry, the same strategy as above was used for integrating GFP, except that instead of a C-terminal fusion, the Gal1 ORF was fully replaced by the GFP by transformation of a PCR product containing a superfolder GFP fused to a Cln2 PEST sequence with a kanMX cassette for selection using oligos OL2306 and OL2079 and plasmid pMaM4 as a template to first create strain RSY14. The kanMX marker in RSY14 was changed to natMX to produce RSY16 by PCR-mediated homologous recombination of natMX amplified by oligos OL2080 and OL2079 from plasmid p4339. Gal3 was then tagged with mCherry by transformation of a PCR product including mCherry with the His5 selection marker using oligos OL2307 and OL2308 and plasmid pKT355 as a template.

High-throughput Gal1 reporter/mutant yeast library construction. The Gal1-GFP reporter query strain (RSY17, mat α, containing natMX for clonNat resistance) was crossed to the SGA single-deletion collection of non-essential genes (Costanzo et al., 2010) to result in a chromatin-focused library containing 567 strains. The SGA library consists of 4,309 BY4741 (MATa *his3Δ1 leu2Δ0 ura3Δ0 met15Δ0*) single knockout strains each carrying deletion of a non-essential gene that is replaced with the antibiotic marker kanMX, which

confers resistance to G418 (Geneticin). In addition to the single-deletion strains, our SGA library contains a control strain in which the kanMX cassette has been inserted at the leu2 locus, specifically between chromosomal position chrIII:84678-92738. Through an automated selection process, diploid cells were sporulated, germinated and passaged as previously described (Costanzo et al., 2010), using a BM3-BC colony-processing robot (S&P Robotis Inc.) to isolate haploids containing both natMX and kanMX for the reporter and deletion cassettes, respectively. Mutants containing the Gal1 reporter in combination with a specific gene deletion were isolated as described (Costanzo et al., 2010), with the following modifications to improve population purity (Kyriakou et al., 2016): a) strains were pinned 2 times (instead of 1) on media selecting for *can1Δ*, *lyp1Δ* and STE2pr-Sp_his5, and b) strains were pinned 2 times (instead of 1) on media selecting for double deletions. After the final selection of haploid strains, a chromatin-focused library was created using a re-array procedure on the BM3-SC robot. Specifically, the library contained 567 yeast strains of which 535 carried deletions of known non-essential chromatin-associated factors, and also included 31 deletion strains that were randomly selected non-chromatin associated factors and 1 control strain in which kanMX was inserted at the leu2 locus. Selected strains were verified by junction PCR to detect the presence of corresponding kanMX and natMX cassettes and absence of WT alleles.

Reconstruction of selected candidates. For validation of their screen phenotypes, RSY208 was transformed with PCR products of kanMX to recreate 30 selected candidate deletion strains by PCR-mediated homologous recombination. Oligonucleotides are listed in Table S2.

Yeast media. Standard yeast media were used. Yeast transformations were done in YPD supplemented with antibiotics for a final concentration of 100 ug/mL clonNat

(Nourseothricin, Jena Bioscience) and/or 500 ug/mL G418 Sulfate (Geneticin, Calbiochem/Merck Millipore). Microfluidics, qPCR, and western experiments were carried out in Synthetic Complete (SC) medium made with dropout mix (US Biological D9515) and YNB + AmSO4 without amino acids (Becton-Dickinson 291940) supplemented with 1.5-2% final concentration of raffinose (raf), glucose (glu), or galactose/raffinose (gal/raf). For these experiments, cells were grown overnight in raf medium, then diluted in raf medium to obtain log phase cultures. Yeast were then subject to memory media change protocols including 4 hrs repression in glu (r1), 1.5-3 hrs induction in gal/raf (i1), followed by a second 4 hr repression in glu (r2) and a second induction in gal/raf (i2), followed by a final repression in glu (r3). Additional media for library construction are as previously described (Tong et al., 2001). Cycloheximide experiments included cycloheximide at a final concentration of 1-2 ug/mL during induction and for 30 min after the change to repression, sufficient time for Gal1 mRNAs to be degraded, ensuring that transcribed RNAs produced in i1 were not translated.

Plasmid construction. Plasmid pY064 was constructed by cloning in a Cln2 PEST degron sequence from pGC05D at the C-terminus of a superfolder GFP in pMaM4. Plasmid pY064 was constructed by cloning in an ~1 kb upstream region of the Ura3 promoter (amplified by oligos OL2089 and OL2090 with genomic DNA from RSY17) into plasmid PL1603 containing the Nab2NLS-2mCherry nuclear marker for homology-directed integration in the Ura3 region in Y7092.

RT-qPCR. RNA was extracted from logarithmically growing yeast (O.D. ~0.5) using the YeaStar RNA kit (Zymo), and purified RNA was digested with Turbo DNAse (Ambion), which was heat inactivated at 65^{o}C for 10 min. cDNA was generated with an oligoDT primer

using the RevertAid first strand cDNA synthesis kit (Thermo). qPCRs were performed using ABsolute Blue qPCR SYBR green mix (Thermo) and cDNA samples with Gal1-specific qPCR primers, oligos OL2091 and OL2092 in a Roche Lightcycler 96 or 480. Gal1 was quantified relative to Tcm1 as a reference gene using the ΔC_T method.

Western blot. At indicated timepoints, an aliquot of cells was removed from logarithmically growing cultures and proteins were extracted in Laemmli SDS buffer(Kushnirov, 2000). Samples were run on 8% polyacrylamide gels, transferred to nitrocellulose, and stained with Ponceau (0.1% Ponceau S (w/v), 5% acetic acid) to control for gel loading. Membranes were blocked with 5% BSA in 1xTBST and probed with primary antibody anti-GFP (Thermo A-11122) in a 1:1000 dilution in 1% BSA, 1xTBST. Secondary antibody anti-rabbit was used at a dilution of 1:100,000 in 1% BSA, 1xTBST and signal visualized by Immobilon (Merck) or Clarity (Bio-Rad) ECL.

Cell-tracking microscopy setup and microfluidics devices. We used a microfluidic device designed to observe single yeast cells through several generations. The chip can accommodate 16 different yeast strains or conditions simultaneously in individual microchambers (Goulev et al., 2017). Each microchamber has 8 microchannels where yeast can be captured, as well as 2 lines for cell injection and 2 major lines for the rapid exchange of media. Phase contrast and fluorescence images of live cells were recorded every 3 min via automated time-lapse microscopy using an inverted microscope (AxioObserver or Nikon Eclipse Ti-E) with epifluorescence capabilities and a temperature-controlled stage (custom-built, IGBMC). For candidate maintenance/inheritance analyses, inductions were fixed to 3 hrs for all strains, long enough to sufficiently induce Gal1 in all strains and observe

differences to the WT, yet short enough for Gal1-GFP to degrade during the repressions, which were fixed to 4 hrs.

Cell-tracking data processing and analysis. We used custom-made PhyloCell and Autotrack softwares (available on Github https://github.com/gcharvin) written in MATLAB (MathWorks) for image segmentation, cell-tracking, fluorescence measurements, and lineage analysis (Goulev et al., 2017).

Gal1 intensity. Gal1-GFP fluorescence was measured and normalized to cell area. Background autofluorescence was calculated by averaging the fluorescence in cell contours over an interval at the beginning of i1 and subtracted from intensity measurements when necessary. Intensities are reported for the end of the induction phase unless otherwise stated.

Gal1 delay. Gal1 delay represents the time difference from the start of galactose exposure until detectable fluorescence. Delay was defined by a positive derivative of Gal1 intensity over 3 frames on smoothed intensity traces (over 4 frames) in order to minimize the effect of spurious intensity fluctuations. Non-inducers with no computed delay were not included in figures displaying delays, including Figures 1D middle and right, 2D, 4A, 4B, 4C, 4E, 4F, and S4B bottom.

Mother and daughter definitions. Nuclear division markers (NLS-tagged mCherry) were used to automatically define relationships between mother cells and their specific daughters and record their birthtime in PhyloCell. Mothers are defined as cells born before i1 and therefore present throughout both inductions. Calculations with daughter cells were restricted to cells born during r2 (born after i1 and before i2), though mothers could give rise to daughters at

other times (not included in our analyses).

Density estimates for delays. Density estimates used a Gaussian kernel with a bandwidth given by Scott's rule as $1/n^5$ where n is the number of data points.

Partial correlations (PCs). PCs (Rummel, 1976) were calculated to measure the degree of association between two cells, while removing the effect of galactose induction that would result in extremely high correlations even among unrelated cells. To subtract this effect, average Gal1 expression in the population was calculated over time and used as the controlling variable. PCs for Gal1 expression over 1 hour of induction were calculated.

Expression rate. Expression rate was approximated by the slope of a line passing through the single-cell expression curve at the time of detected delay and at maximal expression.

Relative difference (RD) of delay. RD was defined as the absolute value of two delays divided by the sum of the delays. RDs were calculated for the time delay until Gal1 expression for each mother to itself in i1 versus i2 or for a pair of mother and daughter cells in i2. To ensure that the effects were specific to mother-daughter pairs and not a general feature of the mutant strain, RDs were also calculated for randomized mothers and daughters using equivalent sample sizes as the related cells; in these randomized pairs, no difference was observed between the strains (data not shown).

Posterior distribution functions. Using Bayesian Statistics, a posterior distribution $P(p|k,N)$ was calculated where p is the probability that the mother expresses before its daughter given the data (k,N):

$$P(p|k,N) = \frac{L(k|p,N) \cdot \pi(p)}{\int L(k|p,N) \cdot \pi(p)dp}$$

Where L is a binomial likelihood, and $\pi(p)$ is a $Beta$ $(1,1)$ flat prior distribution. In this case, we were interested in the probability that mothers express earlier more than 50% of the time. Thus we calculated the posterior probability that p was larger than 0.5 by integrating $P(p|k,N)$ on the interval [0.5,1]. A probability outcome of 0.5 would then indicate that neither mothers nor daughters express earlier than the other group.

Growth rates. Doubling times were calculated according to (Schmidt, 2018). Briefly, total cell area (A) in images at 2 timepoints (t_1 and t_2) was used to determine growth rate with the following equation:

doubling time = $(t_2\text{-}t_1)*\log(2))/(\log(A_{t2})\text{-}\log(A_{t1}))$

High-throughput microfluidics and microscopy setup. For library screening, we used a "microchemostat" microfluidic platform containing an array of 1,152 microchambers each of which can be filled with a different yeast strain, with an integrated valve system to allow for a single flow of medium through the whole array as well as automated media changes (Denervaud et al., 2013). Images were captured at 60x magnification with 10-minute resolution for each strain, and then were segmented and analyzed with a custom platform. Each experiment contained 2 technical replicates for each strain spotted in different locations on the chip to avoid experimental biases, with 3 biological replicates of the screen.

Screen data processing and analysis.

Data measurements. For each strain the mean, median, and standard deviation of Gal1 intensity was monitored over time. All values were collected using the standard background subtraction method and are in arbitrary units. In addition, for each timepoint the percentage of cells that are expressing Gal1 was calculated using an intensity threshold of 150 a.u. When necessary, linear regression was used to adjust for any gradient in nutrients due to diffusion rates through each chemostat.

Quality control. The whole microfluidics device was imaged during overnight growth in raf at 4x magnification. Microchambers that were not completely filled with cells by the start of the memory experiment were excluded from analysis. For quality control within the microfluidics device, any row of cells with markedly different Gal1 expression or growth rate was eliminated from analysis.

Intensity and induction timing analysis of screen data. For Gal1 expression level, we estimated the intensity of GFP fluorescence using a weighted linear fit. The weight w_{TP} was necessary to avoid fitting out-of-focus images and relied on the number of properly defined cells NbC_{TP} from the segmentation at the respective timepoint TP

$$w_{TP} = \frac{NbC^2_{TP}}{50^2 + NbC^2_{TP}}$$

The fit used the data acquired between 30 min before and after the estimated timepoint to include 3 frames for each microchamber. To estimate Gal1 induction timing, we fit a smoothed cubic spline to timepoints after the start of the respective inductions. We used an intensity threshold to identify induced cells in i1 and defined a minimum percentage of

induced cells i_0, using the minimum percentage of expressing cells 1 hr prior to i1 (~0%), or the minimum percentage of expressing cells +/-20 min from the start of i2. If necessary for some strains where not all cells returned to background levels during r2 prior to the start of i2, we additionally used a percentage threshold. The threshold $delT_1$ for delay time was composed of the fixed induced percentage threshold parameter $delT_0$ and the estimated value of induced cell percentage during the beginning of induction a_0

$$delT_1 = i_0 + (1 - i_0) \cdot delT_0$$

We chose an induced cell threshold $delT_0$ of 50% as this represents the median of cells expressing Gal1 and also because the medium shape of the induced cell percentage over time can be approximated by a logistic function, which is the steepest for 50%, making it the threshold with the smallest theoretical estimation error.

Data condensation of screen biological replicates. To allow the merged representation of all 3 experimental repeats, we applied locally weighted scatterplot smoothing (LOESS). We used the mean of repeats from the 3 experiments to compute a local regression curve for each of the 4 data points (intensity and delay during i1 and i2) in each experiment. These curves were then used to standardize all individual microchambers towards an average experiment.

Outlier detection (strains of interest). Our complex dataset justified testing a number of methods for outlier identification. We identified outliers in the 2D distributions of our unmerged and condensed datasets according to intensity and delay values by using a cutoff-based approach to detect strains that are repeatedly different from the norm. First, outlier cutoffs were made for i1 by combining a percentage-based cutoff with an interquartile range

approach. For this, the percentage was set at the 2% and 98% quartile and r for the interquartile range was set as 1, ~2% for a normal distribution. For i2, the data points were first sorted after their i1 values. We then used a moving window of 11 data points combined with the interquartile range to obtain moving thresholds for upper and lower outliers using cubic smoothing splines to get smooth curves for these values.

Candidate validation.

WT reference response curve. To characterize the memory exhibited by the WT as a reference, we measured the peak Gal1 intensities in i1 and i2 for 5 induction lengths ranging from 96 min to 180 min (equal for i1 and i2 within the same experiment), in 13 time-lapse microfluidics experiments with a total of 121 microchamber positions. We characterized the WT memory by determining a response curve which gives the average i2 induction for a given i1 induction, $I2_{\mathrm{ref}}(I1)$, as follows. First we performed a kernel density estimate of the conditional probability $p(I2|I1)$ to observe an average peak i2 induction level $I2$ after average peak i1 level $I1$. We then interpolated its quantiles at 0.5, 0.32 and 0.68 using a smoothing spline, which produced the mean response $I2_{\mathrm{ref}}(I1)$ (solid line in Figure S4A) with lower and upper boundary lines (dashed lines in Figure S4A).

Signed distance to the WT response curve. 30 mutant candidates recreated by PCR-mediated homologous recombination were also induced for induction lengths from 96 to 180 min in 21 microfluidics experiments, covering 106 microchambers with each strain represented in at least 8 microchambers. Candidates were measured for their deviation from the WT response at equivalent induction lengths by calculating a deviation measure for each microchamber containing the strain of interest, given as a Z-score, that is, normalized by the corresponding range of WT variability, as follows:

$$d(I2) = \frac{I2 - I2_{\mathrm{ref}}(I1)}{|I2_{\mathrm{sigma}}(I1) - I2_{\mathrm{ref}}(I1)|},$$

Here, $I2_{\mathrm{sigma}}(I1)$ is the interpolated quantile at 0.32 for $I2 < I2_{\mathrm{ref}}(I1)$ and at 0.68 for $I2 > I2_{\mathrm{ref}}(I1)$, respectively. Lines of equal deviation at $d = \pm 1, \pm 3, \pm 5$ are shown in Figure 3D. To assess whether mutant data fall within or outside the WT range of responses, we compared the measured deviations d of each mutant candidate with those of the WT, using a two-sample Anderson-Darling (AD) test. Candidates were then ranked according to statistical significance based on AD scores.

Mathematical Modeling.

Stochastic delay model. Gal1 promoter activation was modeled as a sequential stepwise process with two parameters (Figure 5B): the number of activation steps n and the rate of each step α, which we assume to be the same for each step for simplicity. The corresponding delay time (i.e. the time needed to reach the active state A from the inactive state I, Figure 5B) is Erlang-distributed with mean n/α. This allows us to quantitatively fit the delay distributions of cells in i2 (Fig. 4B) with a simple Erlang distribution, and likewise the relative difference of mother and daughter cells in i2 (Fig. 4E) with the relative difference of two Erlang-distributed random variables. For fitting, we use the likelihood free pyABC package (Klinger et al., 2018) which allows us to consider both delay and relative difference. Apart from the model, we specify the prior distribution for $n \in [1,20]$ and $\alpha \in [0.1,15]$ 1/min and the distance function. To fit both delay and relative difference, which are on different scales (Figures 4B and 4E), we normalize the mean and the variance of the delay with the mean and variance observed in the data, respectively, and divide the mean and variance of the

delay distribution by the variance of the data and the square root of the number of data points, respectively. The posterior estimates for the parameters show similar rates, but different activation steps. We simulate delay and relative difference with 10 steps for WT and 6 steps for the *elp6Δ* mutant and find that a reduced number of activation steps can explain both reduced delay and at the same time, a larger mother-daughter relative difference (Figure 5D). For implementation details, the Jupyter notebook is available on Github (https://github.com/ccmarr/yeast-delay).

Chromatin immunoprecipitation (ChIP).

ChIP sample collection. Strains were subjected to memory timecourses involving media changes for cycling repressions and inductions and were maintained at OD ~0.5 throughout. For each ChIP timepoint collected, samples were also collected for RT-qPCR to ensure Gal1 was induced and showed memory. For each ChIP timepoint, 9x10^8 cells were crosslinked at room temperature for 30 min with 1% formaldehyde (enough for ~10 IPs). All strains were crosslinked with the same number of cells and volume at each timepoint; when necessary, medium was added to make all cell densities equivalent. Cells were washed 1x with 10 mL cold PBS, 1x with 10 mL cold PBS+histone deacetylase inhibitors (50 mM sodium butyrate and 5 mM nicotinamide), and frozen pellets were stored at -80 deg C.

Chromatin preparation and IPs. Cell pellets were lysed using zirconia beads on a BeadBeater (Biospec) in SDS buffer (50 mM Tris-HCl pH 8.0, 10 mM EDTA, 1% SDS, protease inhibitors, 5 mM nicotinamide, 50 mM sodium butyrate). Supernatants were sonicated (Qsonica) to an average of ~200 bp. Chromatin was diluted with IP buffer (16.7 mM Tris-HCl pH 8.0, 1.2 mM EDTA, 1.1% Triton-X-100, 0.01% SDS, 167 mM NaCl, protease inhibitors, 5 mM nicotinamide, 50 mM sodium butyrate) and then precleared with preblocked

beads and 1/10 was used for each IP. H3 antibody (Abcam ab1791) was incubated with chromatin and IPed with a mixture of IgG and IgA beads. IPs were washed 1x with TSE-150 wash buffer (20 mM Tris-HCl pH 8.0, 2 mM EDTA, 150 mM NaCl, 1% Triton-X-100, 0.1% SDS), 1x with TSE-500 wash buffer (20 mM Tris-HCl pH 8.0, 2 mM EDTA, 150 mM NaCl, 1% Triton-X-100, 0.1% SDS), 1x with LiCl wash buffer (10 mM Tris-HCl pH 8.0, 1 mM EDTA, 1% sodium deoxycholate, 1% NP-40, 250 mM lithium chloride), and a final wash in TE buffer (10 mM Tris-HCl pH 8.0, 1 mM EDTA) before elution with 100 mM sodium bicarbonate and 1% SDS. Samples were reverse crosslinked, treated with RNase A and Proteinase K, then purified (QIAquick PCR purification) and used for qPCR.

ChIP-qPCR. qPCRs were performed using ABsolute Blue qPCR SYBR green mix (Thermo) and ChIP samples with *GAL1* promoter-specific qPCR primers, oligos OL2243 and OL2244, in a Roche Lightcycler 96 or 480. H3 was quantified at the *GAL1* promoter relative to input. H3 ChIPs in mutant strains were normalized to WT within each timepoint.

Nuclease sensitivity.

Nuclease sensitivity sample collection. Samples were collected and digested with micrococcal nuclease (MNase) as previously with minor changes (Bryant et al., 2008). Briefly, WT and *elp6Δ* were subjected to memory timecourses as for ChIP. For each sample, 100 mL of OD 0.5 cells were crosslinked at room temperature for 5 min with 0.5% formaldehyde. Formaldehyde was quenched with final 0.125 M glycine and washed 1x with 10 mL cold PBS and frozen pellets were stored at -80 deg C.

Chromatin preparation and nuclease digestion. Cell pellets were lysed using zirconia beads on the BeadBeater with FA lysis buffer without EDTA (50 mM Hepes-KOH (pH 7.5), 140

mM NaCl, 1% Triton X-100, 0.1% sodium deoxycholate). For each digestion, 26 uL of supernatant was diluted with 120 uL FA lysis buffer without EDTA
and then 10 uL of an MNase solution (Thermo) ranging from 0.125 – 4 units was added with an undigested sample for reference. Digestions were started by adding 5.6 uL of 2 mM $CaCl_2$ and incubated at 37 deg for 1.5 hours. Reactions were quenched with the addition of 8.8 uL 0.5 M EDTA, and SDS and NaCl were added to a final concentration of 1% and 200 mM, respectively. Samples were reverse crosslinked and treated with Proteinase K by incubating at 42 deg for 1 hour followed by 65 deg for at least 4 hours, then purified (QIAquick PCR purification) and used for qPCR.

MNase-qPCR. qPCRs were performed using ABsolute Blue qPCR SYBR green mix (Thermo) and nuclease sensitivity samples with *GAL1* promoter-specific qPCR primers, oligos OL2282 and OL2283, in a Roche Lightcycler 96 or 480. Amplicons in each digested sample are relative to undigested sample Gal1 using the ΔC_T method. Shown is the ratio of WT to *elp6Δ* (where templates were digested with the same MNase concentration within one experiment).

Statistics.

We used t-test, Kolmogorov-Smirnov (KS), Anderson-Darling (AD), and Mann-Whitney *U* (MW) tests to assess statistical significance. For t-test, we used Bonferroni correction for multiple testing. For KS we used two-sided tests, and for Anderson-Darling we used two-sample tests. For MW, we used two-sided non-parametric tests with Bonferroni correction for multiple testing. Box-plot elements are as follows: center line, median; diamond, mean; box limits, upper and lower quartiles; whiskers, 1.5x interquartile range; points, outliers. *P*-value

significances are denoted by ns (not significant)>0.05, * <= 0.05, ** <= 0.01, *** <= 0.001

****<= 0.0001, with exact *P*-values in Supplemental Table S3.

References

Avramova, Z. (2015). Transcriptional 'memory' of a stress: transient chromatin and memory (epigenetic) marks at stress-response genes. The Plant Journal *83*, 149-159.
Berry, S., Dean, C., and Howard, M. (2017). Slow Chromatin Dynamics Allow Polycomb Target Genes to Filter Fluctuations in Transcription Factor Activity. Cell Syst *4*, 445-457 e448.
Brickner, D.G., Cajigas, I., Fondufe-Mittendorf, Y., Ahmed, S., Lee, P.C., Widom, J., and Brickner, J.H. (2007). H2A.Z-mediated localization of genes at the nuclear periphery confers epigenetic memory of previous transcriptional state. PLoS Biology *5*, e81.
Bryant, G.O., Prabhu, V., Floer, M., Wang, X., Spagna, D., Schreiber, D., and Ptashne, M. (2008). Activator control of nucleosome occupancy in activation and repression of transcription. PLoS Biology *6*, 2928-2939.
Cerulus, B., Jariani, A., Perez-Samper, G., Vermeersch, L., Pietsch, J.M., Crane, M.M., New, A.M., Gallone, B., Roncoroni, M., Dzialo, M.C.*, et al.* (2018). Transition between fermentation and respiration determines history-dependent behavior in fluctuating carbon sources. Elife *7*, e39234.
Chen, C., Huang, B., Eliasson, M., Ryden, P., and Bystrom, A.S. (2011). Elongator complex influences telomeric gene silencing and DNA damage response by its role in wobble uridine tRNA modification. PLoS Genetics *7*, e1002258.
Costanzo, M., Baryshnikova, A., Bellay, J., Kim, Y., Spear, E.D., Sevier, C.S., Ding, H., Koh, J.L., Toufighi, K., Mostafavi, S.*, et al.* (2010). The genetic landscape of a cell. Science *327*, 425-431.
D'Urso, A., and Brickner, J.H. (2017). Epigenetic transcriptional memory. Current Genetics *63*, 435-439.
Denervaud, N., Becker, J., Delgado-Gonzalo, R., Damay, P., Rajkumar, A.S., Unser, M., Shore, D., Naef, F., and Maerkl, S.J. (2013). A chemostat array enables the spatio-temporal analysis of the yeast proteome. Proceedings of the National Academy of Sciences of the United States of America *110*, 15842-15847.
Esberg, A., Huang, B., Johansson, M.J., and Bystrom, A.S. (2006). Elevated levels of two tRNA species bypass the requirement for elongator complex in transcription and exocytosis. Molecular Cell *24*, 139-148.
Floer, M., Wang, X., Prabhu, V., Berrozpe, G., Narayan, S., Spagna, D., Alvarez, D., Kendall, J., Krasnitz, A., Stepansky, A.*, et al.* (2010). A RSC/nucleosome complex determines chromatin architecture and facilitates activator binding. Cell *141*, 407-418.
Foster, S.L., Hargreaves, D.C., and Medzhitov, R. (2007). Gene-specific control of inflammation by TLR-induced chromatin modifications. Nature *447*, 972-978.
Francis, N.J., and Kingston, R.E. (2001). Mechanisms of transcriptional memory. Nature reviews Molecular cell biology *2*, 409-421.
Goulev, Y., Morlot, S., Matifas, A., Huang, B., Molin, M., Toledano, M.B., and Charvin, G. (2017). Nonlinear feedback drives homeostatic plasticity in H2O2 stress response. Elife *6*.

Halley, J.E., Kaplan, T., Wang, A.Y., Kobor, M.S., and Rine, J. (2010). Roles for H2A.Z and its acetylation in GAL1 transcription and gene induction, but not GAL1-transcriptional memory. PLoS Biology *8*, e1000401.
Iberg-Badeaux, A., Collombet, S., Laurent, B., van Oevelen, C., Chin, K.K., Thieffry, D., Graf, T., and Shi, Y. (2017). A Transcription Factor Pulse Can Prime Chromatin for Heritable Transcriptional Memory. Molecular and Cellular Biology *37*.
Keren, L., van Dijk, D., Weingarten-Gabbay, S., Davidi, D., Jona, G., Weinberger, A., Milo, R., and Segal, E. (2015). Noise in gene expression is coupled to growth rate. Genome research *25*, 1893-1902.
Kim, K.S., Rosenkrantz, M.S., and Guarente, L. (1986). Saccharomyces cerevisiae contains two functional citrate synthase genes. Molecular and Cellular Biology *6*, 1936-1942.
Kim, T., Xu, Z., Clauder-Munster, S., Steinmetz, L.M., and Buratowski, S. (2012). Set3 HDAC mediates effects of overlapping noncoding transcription on gene induction kinetics. Cell *150*, 1158-1169.
Klinger, E., Rickert, D., and Hasenauer, J. (2018). pyABC: distributed, likelihood-free inference. Bioinformatics *34*, 3591-3593.
Krogan, N.J., and Greenblatt, J.F. (2001). Characterization of a six-subunit holo-elongator complex required for the regulated expression of a group of genes in Saccharomyces cerevisiae. Molecular and Cellular Biology *21*, 8203-8212.
Kundu, S., Horn, P.J., and Peterson, C.L. (2007). SWI/SNF is required for transcriptional memory at the yeast GAL gene cluster. Genes & Development *21*, 997-1004.
Kundu, S., and Peterson, C.L. (2009). Role of chromatin states in transcriptional memory. Biochim Biophys Acta *1790*, 445-455.
Kundu, S., and Peterson, C.L. (2010). Dominant role for signal transduction in the transcriptional memory of yeast GAL genes. Molecular and Cellular Biology *30*, 2330-2340.
Kushnirov, V.V. (2000). Rapid and reliable protein extraction from yeast. Yeast *16*, 857-860.
Kyriakou, D., Stavrou, E., Demosthenous, P., Angelidou, G., San Luis, B.J., Boone, C., Promponas, V.J., and Kirmizis, A. (2016). Functional characterisation of long intergenic non-coding RNAs through genetic interaction profiling in Saccharomyces cerevisiae. BMC biology *14*, 106.
Li, Q., Fazly, A.M., Zhou, H., Huang, S., Zhang, Z., and Stillman, B. (2009). The elongator complex interacts with PCNA and modulates transcriptional silencing and sensitivity to DNA damage agents. PLoS Genetics *5*, e1000684.
Lohr, D., Venkov, P., and Zlatanova, J. (1995). Transcriptional regulation in the yeast GAL gene family: a complex genetic network. FASEB J *9*, 777-787.
Otero, G., Fellows, J., Li, Y., de Bizemont, T., Dirac, A.M., Gustafsson, C.M., Erdjument-Bromage, H., Tempst, P., and Svejstrup, J.Q. (1999). Elongator, a multisubunit component of a novel RNA polymerase II holoenzyme for transcriptional elongation. Molecular Cell *3*, 109-118.
Rahl, P.B., Chen, C.Z., and Collins, R.N. (2005). Elp1p, the yeast homolog of the FD disease syndrome protein, negatively regulates exocytosis independently of transcriptional elongation. Molecular Cell *17*, 841-853.
Rummel, R. (1976). Understanding Correlation.
Santisteban, M.S., Hang, M., and Smith, M.M. (2011). Histone variant H2A.Z and RNA polymerase II transcription elongation. Molecular and Cellular Biology *31*, 1848-1860.

Schmidt, G.W., Cuny, A. P., Rudolf, F. (2018). Preventing photomorbidity in long-term multi-color fuorescence imaging of S. cerevisiae and S. pombe. bioRxiv *doi: 10.1101/180018.*
Sood, V., and Brickner, J.H. (2017). Genetic and Epigenetic Strategies Potentiate Gal4 Activation to Enhance Fitness in Recently Diverged Yeast Species. Current Biology *27*, 3591-3602 e3593.
Sood, V., Cajigas, I., D'Urso, A., Light, W.H., and Brickner, J.H. (2017). Epigenetic Transcriptional Memory of GAL Genes Depends on Growth in Glucose and the Tup1 Transcription Factor in Saccharomyces cerevisiae. Genetics *206*, 1895-1907.
Stockwell, S.R., Landry, C.R., and Rifkin, S.A. (2015). The yeast galactose network as a quantitative model for cellular memory. Mol Biosyst *11*, 28-37.
Stockwell, S.R., and Rifkin, S.A. (2017). A living vector field reveals constraints on galactose network induction in yeast. Molecular Systems Biology *13*, 908.
Svejstrup, J.Q. (2007). Elongator complex: how many roles does it play? Curr Opin Cell Biol *19*, 331-336.
Tong, A.H., Evangelista, M., Parsons, A.B., Xu, H., Bader, G.D., Page, N., Robinson, M., Raghibizadeh, S., Hogue, C.W., Bussey, H.*, et al.* (2001). Systematic genetic analysis with ordered arrays of yeast deletion mutants. Science *294*, 2364-2368.
Villeneuve, L.M., Reddy, M.A., and Natarajan, R. (2011). Epigenetics: deciphering its role in diabetes and its chronic complications. Clin Exp Pharmacol Physiol *38*, 451-459.
Winkler, G.S., Kristjuhan, A., Erdjument-Bromage, H., Tempst, P., and Svejstrup, J.Q. (2002). Elongator is a histone H3 and H4 acetyltransferase important for normal histone acetylation levels in vivo. Proceedings of the National Academy of Sciences of the United States of America *99*, 3517-3522.
Wittschieben, B.O., Otero, G., de Bizemont, T., Fellows, J., Erdjument-Bromage, H., Ohba, R., Li, Y., Allis, C.D., Tempst, P., and Svejstrup, J.Q. (1999). A novel histone acetyltransferase is an integral subunit of elongating RNA polymerase II holoenzyme. Molecular Cell *4*, 123-128.
Zacharioudakis, I., Gligoris, T., and Tzamarias, D. (2007). A yeast catabolic enzyme controls transcriptional memory. Current Biology *17*, 2041-2046.
Zhou, B.O., and Zhou, J.Q. (2011). Recent transcription-induced histone H3 lysine 4 (H3K4) methylation inhibits gene reactivation. The Journal of Biological Chemistry *286*, 34770-34776.

Figure 1.

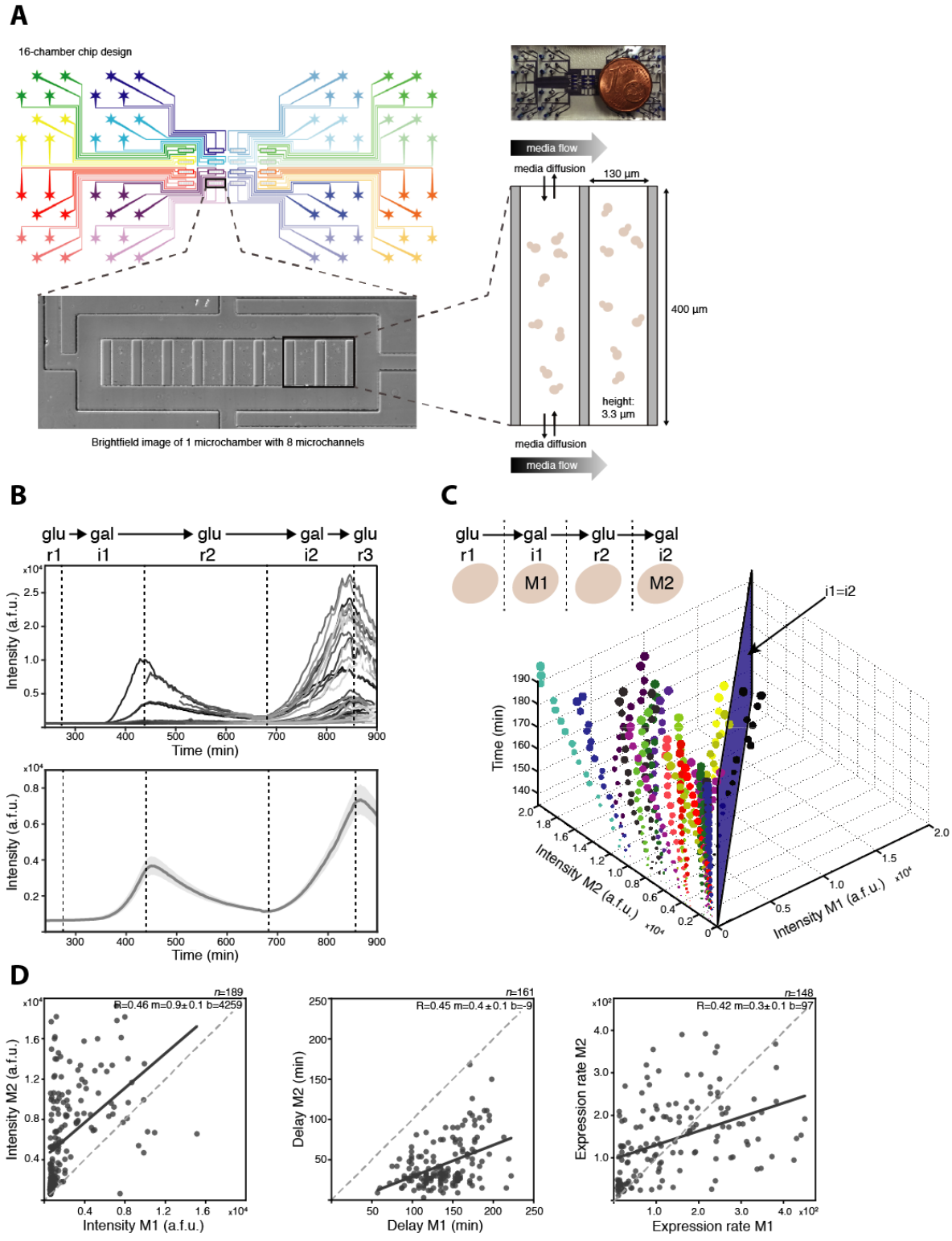

Figure 1. Quantification of Gal1 memory in single cells over time.

A, Cell- and lineage-tracking microfluidics chip design. The chip is designed with 16 fully independent microchambers to allow up to 16 different strains/conditions to be measured

simultaneously with precise time-controlled media changes. Each microchamber contains 8 microchannels where individual yeast cells can be trapped and maintained in a single plane during growth, enabling subsequent segmentation and expression quantification. The design is compatible with both phase contrast and fluorescence imaging of individual yeast cells with cell- and lineage-tracking for at least 7 cell divisions.

B, **top**, Single-cell traces of Gal1-GFP intensity. Yeast cells were subjected to repeated galactose inductions (gal; i1 and i2 = induction 1 and 2, respectively) and glucose repressions (glu; r1, r2, and r3 = repression 1, 2, and 3, respectively) during a memory timelapse imaging experiment using single cell-tracking microfluidics. Individual cells have Gal1 memory, i.e. they express more Gal1 in i2 compared to i1 (representative experiment) **bottom**, Gal1 expression population mean (solid line) ±95% confidence intervals (shaded area), shows that on average the population (including progeny) shows Gal1 memory.

C, Single mother cells express more Gal1 at each timepoint during i2 in comparison with the corresponding timepoint in i1. M1 and M2 = the same mother cell in i1 and i2, respectively. Each color represents a single mother, with increasing dot size according to time from induction start. Any timepoint for each cell that falls to the left of the i1 = i2 plane indicates memory (representative experiment).

D, **left**, 93% of mother cells have memory according to Gal1 intensity at induction end. M1 and M2 = the same mother cell in i1 and i2, respectively. **middle**, 100% of mother cells have memory according to delay until detectable Gal1 expression. **right**, Gal1 expression rate (see Methods) in wild-type (WT) mother cells is similar during i1 and i2. WT mother memory maintenance is due to shorter delay, not increased expression rate, which results in increased intensity in i2. For statistical tests and *P*-values see Table S3.

Figure 2.

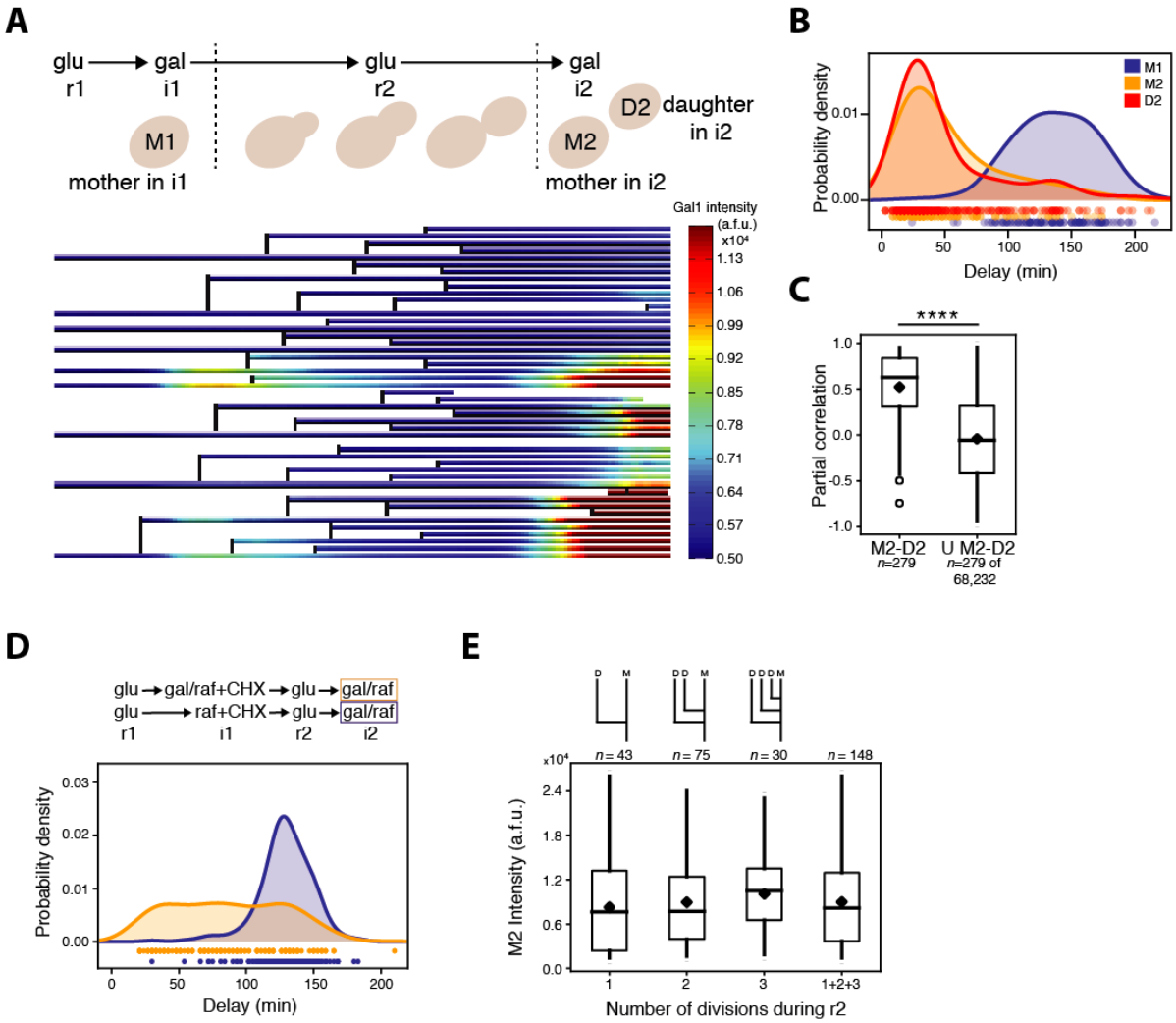

Figure 2. Gal1 memory maintenance in mother cells and inheritance to daughter cells.

A, Gal1 intensity heatmap overlayed on a pedigree shows similar expression patterns between related cells. Mother induction is detected during both i1 and i2 (M1 and M2, respectively), while only galactose-naïve daughters born during r2 are analyzed for inheritance in i2.

B, Unexposed progeny inherit Gal1 memory from pre-exposed mothers according to Gal1 delay. Galactose-naïve daughters (D2, *n*=326) born from pre-exposed mothers have significantly shorter delays in i2 than their mothers in i1 (M1, *n*=122), and are indistinguishable from their mothers in i2 (M2, *n*=140), indicating memory inheritance.

C, Related pairs of cells within the same induction (i2) behave more similarly than unrelated cells. To remove the general trend of Gal1 induction, partial correlations (PCs) were calculated. Significantly higher (63%) PCs between related pairs of mothers and daughters during i2 (M2-D2) compared to unrelated (0%, U M2-D2) indicates Gal1 expression is well correlated over many timepoints and memory is inherited by daughter cells.

D, Protein synthesis during the initial galactose induction (i1) is not solely responsible for memory. WT yeast were grown in a microfluidics device in raf (non-inducing control, *n*=216) or gal/raf medium (*n*=177) during i1 in the presence of cycloheximide (CHX) to prevent translation. Following glu repression (r2), all cells were induced with gal/raf in i2. Delays until Gal1 expression in i2 shows that cells previously exposed to gal reinduce significantly faster than cells naïve for gal, even if translation is blocked in i1.

E, Cell division does not decrease mother memory. Intensity distribution of mother intensities in i2 (M2) is not different between mothers that have divided 1, 2, or 3 times (maximum 3 progeny can be born during r2), demonstrating that cell division does not significantly decrease mother memory. For statistical tests and *P*-values see Table S3.

Figure 3.

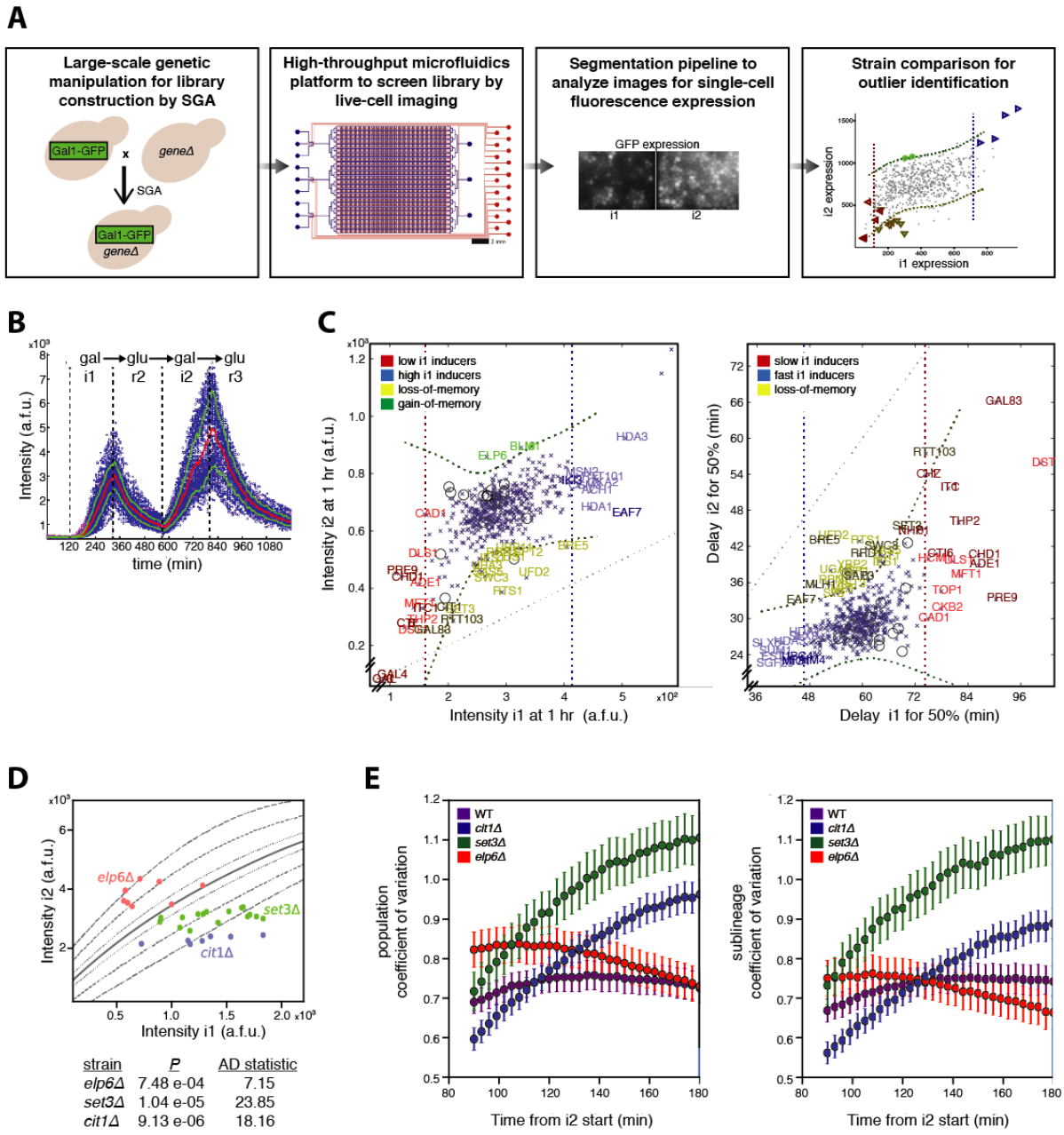

Figure 3. Identification of loss- and gain-of-memory mutants through a novel workflow for high-throughput screening.

A, Workflow of screening includes production of a library of strains harboring a single gene deletion and the reporter of interest using the high-throughput SGA system of library construction (panel 1). The strains are then screened in high throughput using a microfluidics device with 1,152 chambers for automated control of media changes (panel 2). Images are

processed with an automated segmentation and analysis pipeline (panel 3) to identify outliers of interest (dashed lines indicate outlier thresholds, panel 4). The high capacity of the microfluidics chip allowed us to test all strains in duplicate simultaneously with 3 biological replicates.

B, Profile of WT in a high-throughput microfluidics experiment shows memory in the setup. Blue circles represent fluorescence in single cells. Red and green lines represent median and quartiles, respectively.

C, Detection of outliers of Gal1 memory (yellow and green) according to intensity and population expression delay. Crosses represent individual yeast strains with the Gal1-GFP reporter and a single gene deletion. Open circles represent WT replicates. Dashed lines indicate outlier thresholds. Specifically, Gal1 memory outliers are defined as those that are found within the two vertical dashed lines in i1, but outside of the two horizontal dashed lines in i2. **left**, Outliers according to mean Gal1 intensity in i1 and i2. Representative outlier plot 1 hour after induction start in i1 and i2. **right**, Outliers according to population expression delay (time until 50% of the population is expressing detectable Gal1).

D, Comparison of mutants with memory observed in WT yeast at matched induction strengths verifies loss- and gain-of-memory candidates. Lines represent WT induction in i1 and i2 as induction length is varied: mean induction (solid line) and quantile contour lines quantifying variability (dashed lines). Dots represent average induction strengths in i1 and i2 in individual mutant experiments. Anderson-Darling (AD) test statistics confirm that the mutants deviate significantly from the mean WT induction (see Methods).

E, **left**, WT and *elp6Δ* have markedly lower variability (coefficient of variation) in Gal1 expression dynamics than *set3Δ* and *cit1Δ*. Circles indicate mean and error bars SD from bootstrapping (x1000). **right**, Increased Gal1 delay is a feature of some loss-of-memory cell lineages, resulting in high variability (coefficient of variation) between sublineages

particularly within *set3Δ* but also in *cit1Δ* during i2. For statistical tests and *P*-values see Table S3.

Figure 4.

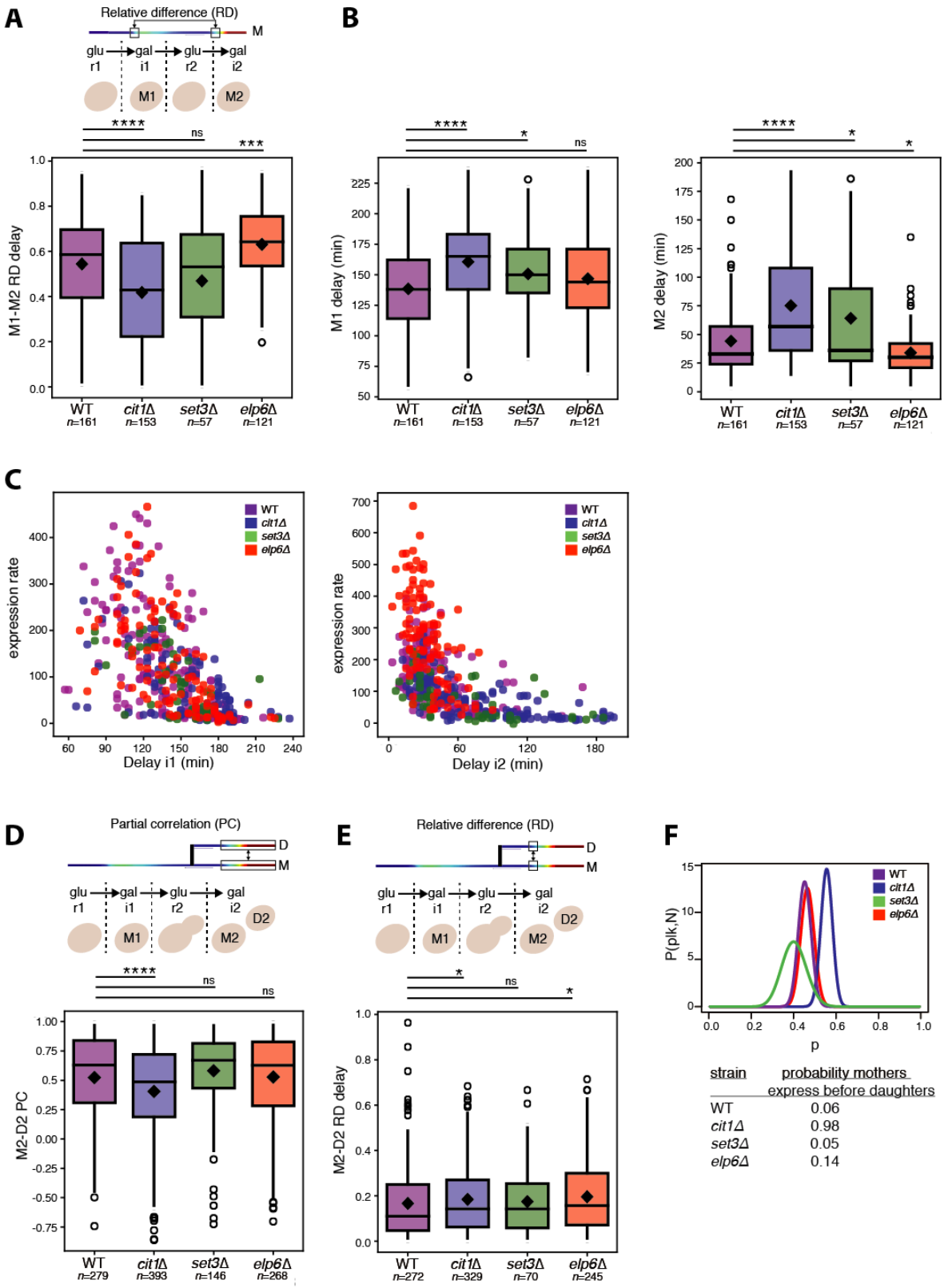
A
Relative difference (RD)
M
glu r1
gal i1
glu r2
gal i2
M1
M2
M1-M2 RD delay
B
M1 delay (min)
M2 delay (min)
WT n=161
cit1Δ n=153
set3Δ n=57
elp6Δ n=121
C
expression rate
Delay i1 (min)
Delay i2 (min)
WT
cit1Δ
set3Δ
elp6Δ
D
Partial correlation (PC)
D2
M2-D2 PC
WT n=279
cit1Δ n=393
set3Δ n=146
elp6Δ n=268
E
Relative difference (RD)
M2-D2 RD delay
WT n=272
cit1Δ n=329
set3Δ n=70
elp6Δ n=245
F
P(plk,N)
p
strain
probability mothers express before daughters
WT 0.06
cit1Δ 0.98
set3Δ 0.05
elp6Δ 0.14

Figure 4. Dissection of mutant effects on maintenance and inheritance of Gal1 memory.

A, Loss- and gain-of-memory mutants affect maintenance of mother memory. M1-M2 relative difference (RD) in the delay reveals that loss-of-memory mutant *cit1Δ* has significantly lower RD than WT while gain-of-memory *elp6Δ* is significantly higher, indicating that these phenotypes are at least in part due to an effect on maintenance of mother memory from i1 to i2.

B, **left**, Loss-of-memory *set3Δ* and *cit1Δ* have longer delays than WT in i1. Gain-of-memory *elp6Δ*, however, has similar delays to WT in i1. **right**, *elp6Δ* has shorter delays in i2, while *set3Δ* and *cit1Δ* have longer delays in i2 than WT.

C, **left**, Comparison of expression rates of cells with similar delays shows no major differences between mutants and WT in i1. **right**, Comparison of *elp6Δ* cells with similar delays as WT reveals an increased expression rate in i2.

D, *cit1Δ* is the only strain with lower M2-D2 partial correlation (PC) in i2 in comparison to WT. Low M2-D2 PC in *cit1Δ* suggests mothers and daughters do not share the same memory.

E, Increased M2-D2 relative differences (RD) in *cit1Δ* and *elp6Δ* in comparison to WT reveals higher variability between mothers and daughters.

F, Posterior distribution functions (P(p|k,N) of strains to determine bias towards mothers expressing earlier than daughters in i2 (p). Shown are the probabilities (P(p|k,N) that a deviation from neither mother nor daughter expressing first (p = 0.5) is significant. *cit1Δ* shows a 98% probability that mothers express before daughters (p > 0.5), while in all other strains the probability for such preference is negligible, suggesting that *cit1Δ* has a defect in inheritance of memory. For statistical tests and *P*-values see Table S3.

Figure 5.

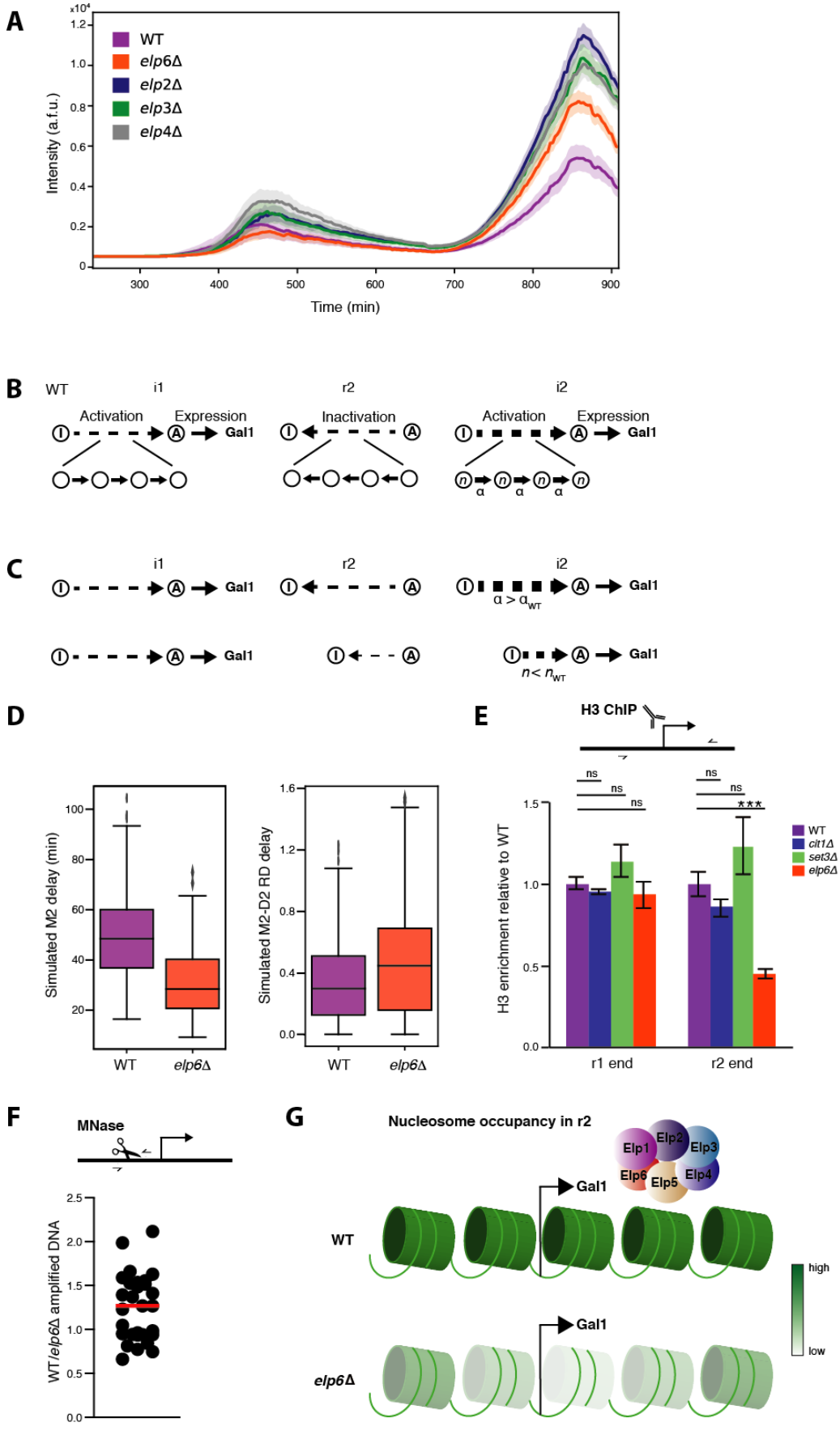
A
WT
elp6Δ
elp2Δ
elp3Δ
elp4Δ
Intensity (a.f.u.)
Time (min)
B
WT
i1
r2
i2
Activation
Expression
Inactivation
Gal1
C
i1
r2
i2
Gal1
α > α_WT
n< n_WT
D
Simulated M2 delay (min)
Simulated M2-D2 RD delay
WT
elp6Δ
E
H3 ChIP
ns
***
H3 enrichment relative to WT
WT
cit1Δ
set3Δ
elp6Δ
r1 end
r2 end
F
MNase
WT/elp6Δ amplified DNA
G
Nucleosome occupancy in r2
Elp1
Elp2
Elp3
Elp4
Elp5
Elp6
Gal1
WT
elp6Δ
high
low

Figure 5. Analysis of *elpΔ*-mediated gain-of-memory effect.

A, Deletion of individual Elp complex members results in gain-of-memory. Shown are Gal1 expression population means (solid lines) ±95% confidence intervals (shaded areas) from microfluidics data of single Elp complex member deletions. Deletion of Elp2, Elp3, or Elp4 recapitulates the gain-of-memory results observed in *elp6Δ*, indicating that gain-of-memory results from a dysfunctional Elp complex.

B, Delay model. Induced cells in i1 transition from an inactive Gal1 promoter state (I) to an active state (A) in sequential steps, leading to Gal1 expression. During repression (r2), the Gal1 promoter is inactivated. Shorter WT delay can be envisioned as coming from an increased activation rate α.

C, Gain-of-memory hypotheses predict shorter delays due to (i) faster activation rates ($\alpha > \alpha_{WT}$) or (ii) less activation steps ($n < n_{WT}$).

D, Fitting a stochastic delay model to the single-cell data shows that less activation steps with unchanged activation rates can explain both a shorter delay and a broader mother-daughter relative difference distribution in i2, as observed for the *elp6Δ* gain-of-memory phenotype (Figure 4B and 4E).

E, ChIP reveals decreased histone H3 enrichment at the *GAL1* promoter in *elp6Δ* at the end of r2. Samples were collected at the end of r1 and r2 and H3 IPs at the Gal1 promoter (arrow = TSS) were quantified by qPCR, with mutants normalized to WT. Error bars indicate SD for 2 technical replicates each from 2 biological replicates, representative experiments verified by 3 additional biological replicates.

F, Nuclease sensitivity assays show higher susceptibility to MNase digestion in *elp6Δ* compared to WT at the end of r2. Samples were collected at the end of r2, digested with MNase, followed by amplification of protected DNA by qPCR. Individual dots represent the ratio of WT to *elp6Δ* amplified DNA. Shown are 29 digestions from 4 biological replicates

with the median ratio (1.27) represented by the red bar. The higher median ratio of WT to *elp6Δ* indicates that the *elp6Δ* samples contain less protected DNA than WT, and that *elp6Δ* chromatin at the Gal1 promoter at the end of r2 is more susceptible to MNase digestion. **G,** Schematic for proposed gain-of-memory mechanism in Elongator mutants by reduced nucleosome occupancy during repression in r2, resulting in faster reinduction in i2. For statistical tests and *P*-values see Table S3.

Figure 6.

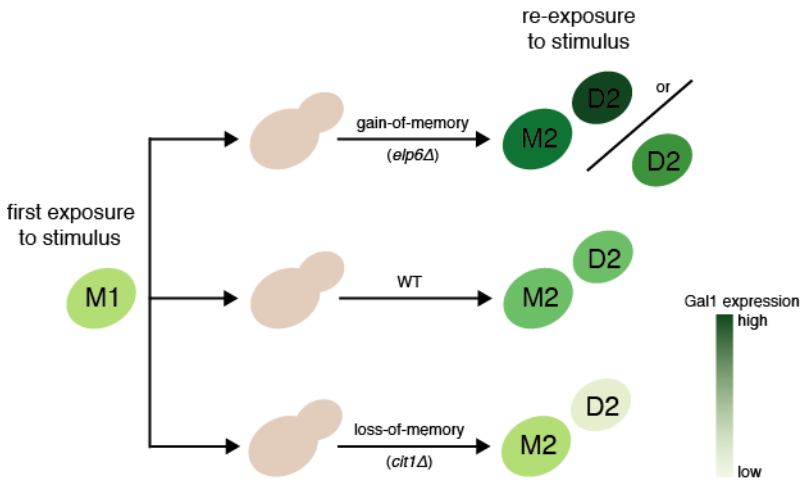

Figure 6. Schematic highlighting identified defects in maintenance and inheritance of memory.

WT mother (M) cells establish and maintain a transcriptional memory during exposure to a stimulus (galactose) resulting in higher expression (indicated by darker color) during re-exposure. Unexposed daughter cells (D) inherit a memory potential similar to that of their mothers. The mutants identified in our screen have different effects on maintenance and inheritance of memory. Gain-of-memory in *elp6Δ* results in increased mother memory, and while *elp6Δ* daughters also generally have gain-of-memory compared to WT cells, there is variability in memory inheritance from their mothers. On the other hand, *cit1Δ* loss-of-memory results in decreased mother memory, with an even stronger phenotype in daughters, resulting in a pattern of asymmetric memory.

Figure S1.

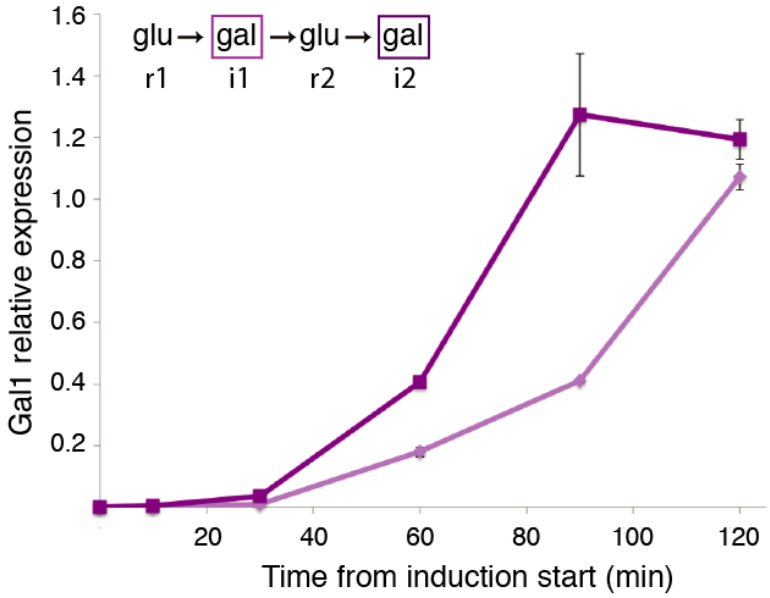

Figure S1. Gal1 memory validated at the RNA level.

RT-qPCR analysis of RNA isolated during galactose inductions from WT yeast cultures during a timecourse memory experiment shows higher amounts of Gal1 mRNA at corresponding timepoints during i2 compared to i1, validating that memory is observed in this strain. Error bars are calculated as SD from 2 technical replicates, shown is a representative experiment verified by 4 biological replicates.

Figure S2.

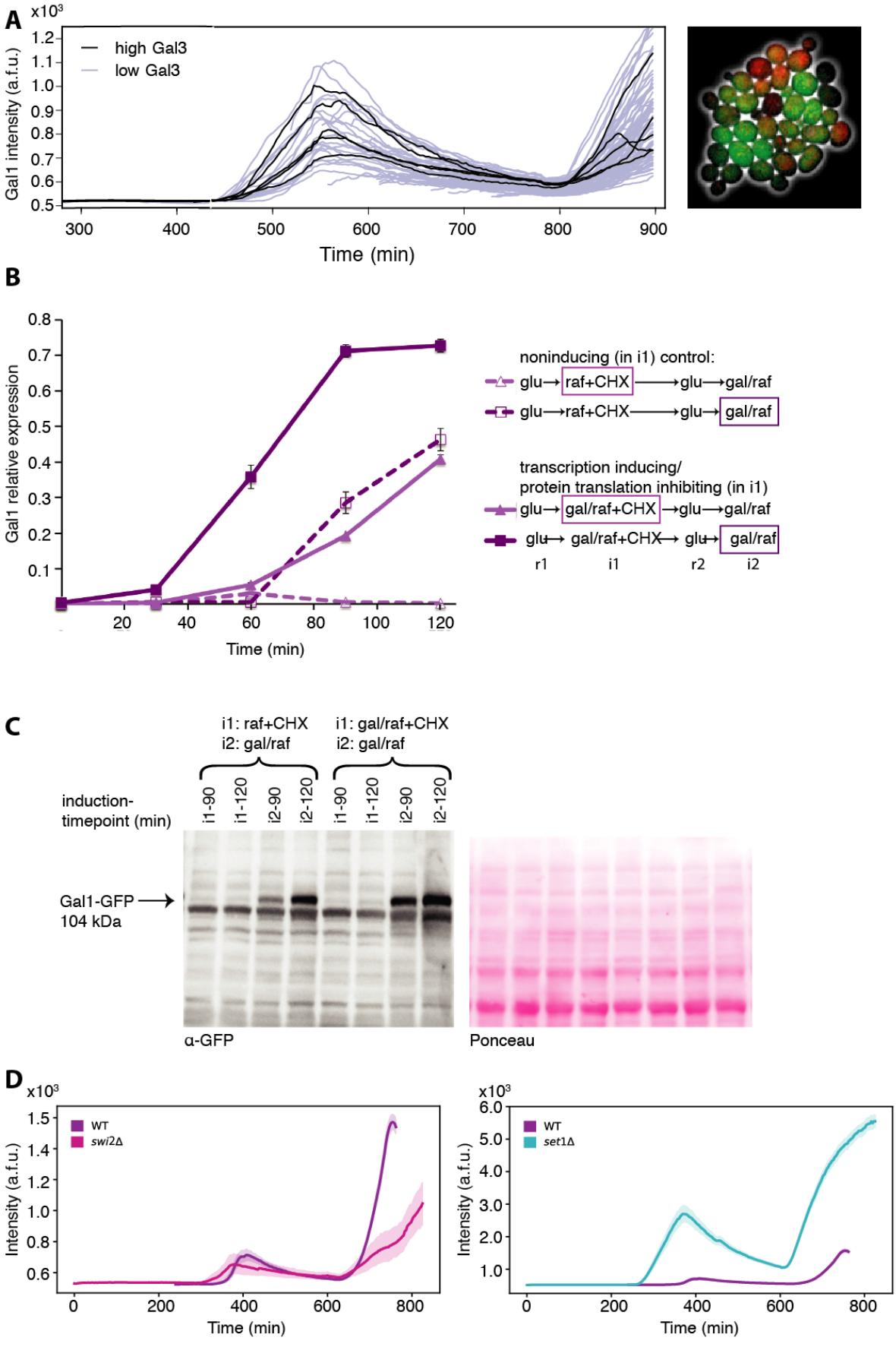
A
x10³
Gal1 intensity (a.f.u.)
high Gal3
low Gal3
Time (min)
B
Gal1 relative expression
Time (min)
noninducing (in i1) control:
glu→ raf+CHX ⟶glu⟶gal/raf
glu⟶raf+CHX⟶glu→ gal/raf
transcription inducing/
protein translation inhibiting (in i1)
glu→ gal/raf+CHX →glu⟶gal/raf
glu→ gal/raf+CHX⟶ glu→ gal/raf
r1 i1 r2 i2
C
i1: raf+CHX
i2: gal/raf
i1: gal/raf+CHX
i2: gal/raf
induction-
timepoint (min)
i1-90
i1-120
i2-90
i2-120
Gal1-GFP
104 kDa
α-GFP
Ponceau
D
x10³
Intensity (a.f.u.)
WT
swi2Δ
Time (min)
x10³
Intensity (a.f.u.)
WT
set1Δ
Time (min)

Figure S2. Protein inheritance and setup validation for Gal1 memory.

A, Gal1 and Gal3 proteins are not essential for memory. Gal1 ORF was replaced with GFP and Gal3 was tagged with mCherry. **left**, Single-cell traces of GFP expressed from Gal1 promoter (blue and black). Cells that display faster reinduction of GFP from the Gal1 promoter are not the ones with the highest Gal3 protein levels prior to reinduction (black). **right**, Representative image during reinduction shows cells with highest Gal3-mCherry do not have the most GFP expressed from Gal1 reporter.

B, Protein translation inhibition by cycloheximide (CHX) during an initial induction does not abrogate memory. RT-qPCR of Gal1 mRNA from cultures of WT yeast grown during i1 in either raf with CHX (non-inducing control) or gal/raf with CHX, subsequently grown during r2 in glu, followed by induction in gal/raf shows Gal1 transcriptional memory in i2 even after protein translation inhibition during i1. Error bars indicate SD from 2 technical replicates.

C, Validation of Gal1 reinduction memory by detecting GFP levels. Immunoblot with a GPF-specific antibody of the same cultures as in (B) shows Gal1-GFP protein expression memory in i2 even after protein translation inhibition during i1.

D, Effect of previously identified mutants implicated in Gal1 memory observed by microfluidics. **left**, Swi2 deletion results in loss-of-memory in comparison to WT. **right**, Set1 deletion results in an increase in Gal1 expression in both inductions. Shown is average Gal1-GFP expression (solid line) ±95% confidence intervals (shaded area).

Figure S3.

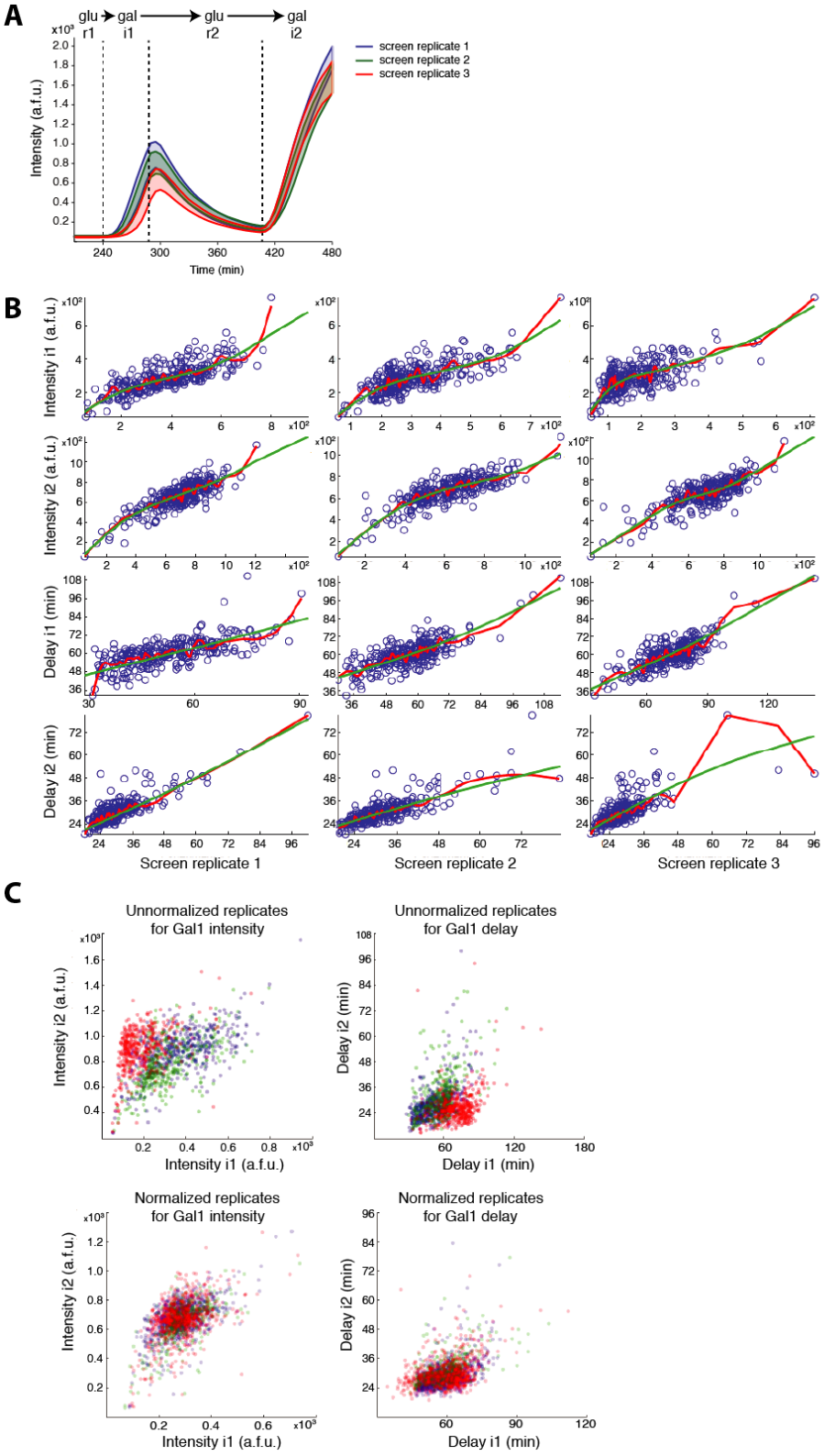
A
glu r1
gal i1
glu r2
gal i2
screen replicate 1
screen replicate 2
screen replicate 3
Intensity (a.f.u.)
Time (min)
B
Intensity i1 (a.f.u.)
Intensity i2 (a.f.u.)
Delay i1 (min)
Delay i2 (min)
Screen replicate 1
Screen replicate 2
Screen replicate 3
C
Unnormalized replicates for Gal1 intensity
Unnormalized replicates for Gal1 delay
Normalized replicates for Gal1 intensity
Normalized replicates for Gal1 delay
Intensity i2 (a.f.u.)
Intensity i1 (a.f.u.)
Delay i2 (min)
Delay i1 (min)

Figure S3. High-throughput microfluidics screen data normalization.

A, Summary of all screen experiments shows reproducibility of the screen. Median and 25 to 75 percentiles of Gal1-GFP intensity for all strains in a single experiment combined is shown for 3 biological screen replicates, each containing technical duplicates.

B, Normalization of screen replicates using LOESS for data reduction. Data collected from 3 independent microfluidics experiments were condensed to a single dataset using LOESS. y-axis shows average values of strains in intensity and delay for both i1 and i2. x-axis shows the respective values in the experimental repeats. Red lines show the result of LOESS, green lines show the final local regression lines used for data normalization.

C, Overlay of screen replicates before and after normalization by LOESS. **top**, raw values for Gal1 intensity and delay. **bottom**, normalized values.

Figure S4.

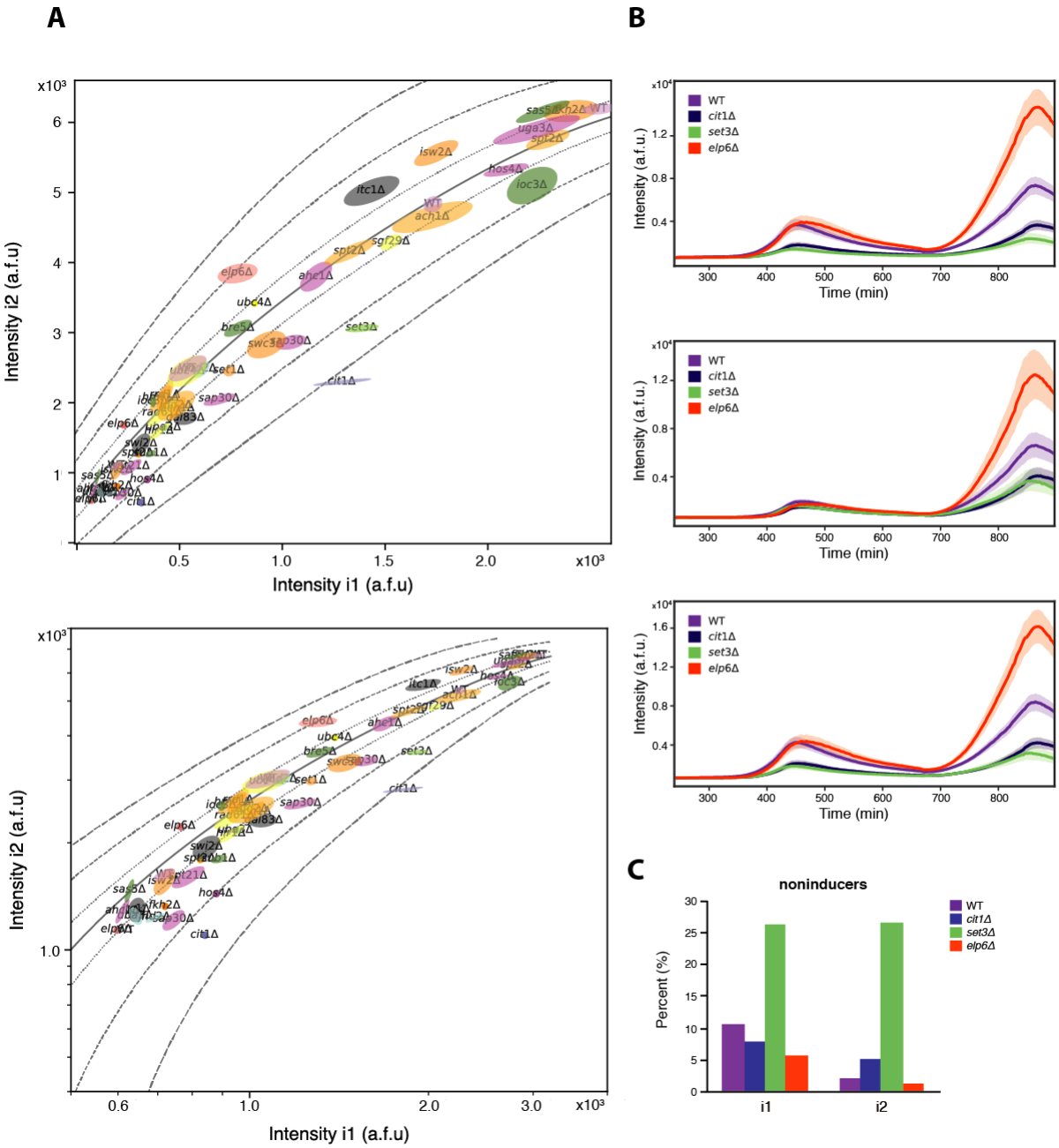

Figure S4. Validation of loss-of-memory and gain-of-memory candidates.

A, Summary of candidate validation experiment results using cell-tracking microfluidics. Individual strains are plotted as maximum Gal1 intensity of cells during induction averaged over all cells in a microfluidics channel, taken from 21 experiments with each strain analyzed in a minimum of 8 microchannels. WT and mutant strains were induced for various lengths of time to minimize the effect of a mutation on overall gene induction strength by achieving

comparable i1 expression. The interpolated WT response curve for different induction lengths is shown as a solid line. Lines of equal deviation from the WT are also shown at deviation Z-score values ±1, ±3 and ±5 (above and below the WT response curve, respectively). The best candidates were identified based on the difference in distribution using two-sample AD tests comparing WT and mutant Z-scores with >200 cells (see Methods). **top**, linear scale. **bottom**, log scale.

B, Removal of non-inducers and thresholding candidate mutant cells does not change the loss-of-memory/gain-of-memory phenotype of candidates. **top**, all data included. **middle,** thresholding cells for each strain for similar expression as WT in i1 shows that the loss-of-memory/gain-of-memory phenotypes of candidates in i2 persist. **bottom**, removing non-inducers from mutant data also shows that the loss-of-memory and gain-of-memory phenotypes persist. Shown are Gal1 expression population means (solid lines) in each of the mutants ±95% confidence intervals (shaded areas).

C, Loss-of-memory mutant *set3Δ* has a high percentage of non-inducers in the population. Box plot of percentage of non-inducer cells for each strain in i1 and i2.

Figure S5.

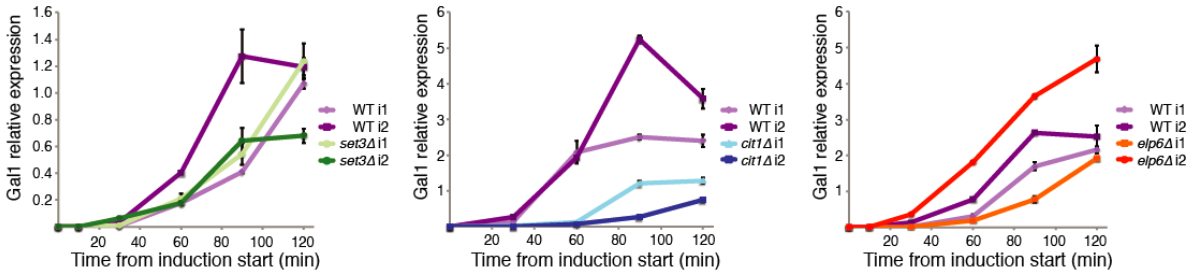

Figure S5. Candidates affect memory at the RNA level.

Mutant memory effects observed at the protein level by GFP are recapitulated at the Gal1 transcript level. RT-qPCR analysis of RNA isolated from indicated candidate strains during timecourse memory experiments. Each strain was tested with a minimum of 4 biological replicates, shown are representative expression profiles. Error bars calculated as SD from 2 technical replicates.

Figure S6.

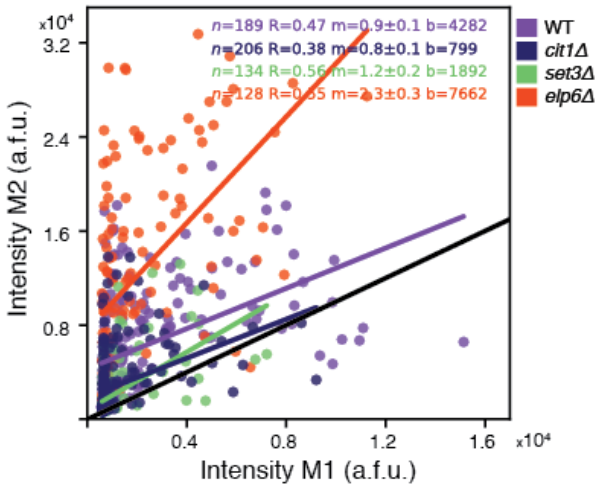

Figure S6. Gal1 memory maintenance effects in mothers.

Scatter plots of Gal1 intensity with linear regressions M2=m*M1+b. Shorter delays of activation manifest as a non-zero offset b (>0) in WT, with no effect on the slope m (~1), which is dominated by changes in expression rates. The gain-of-memory mutant *elp6Δ* reveals an increase in offset and slope compared to WT, likely affecting both activation and expression. Loss-of-memory mutants *set3Δ* and *cit1Δ* have lower offsets compared to WT, demonstrating an impact on activation and resulting in loss-of-memory. This suggests that different steps leading to Gal1 expression are affected in the mutants.

Figure S7.

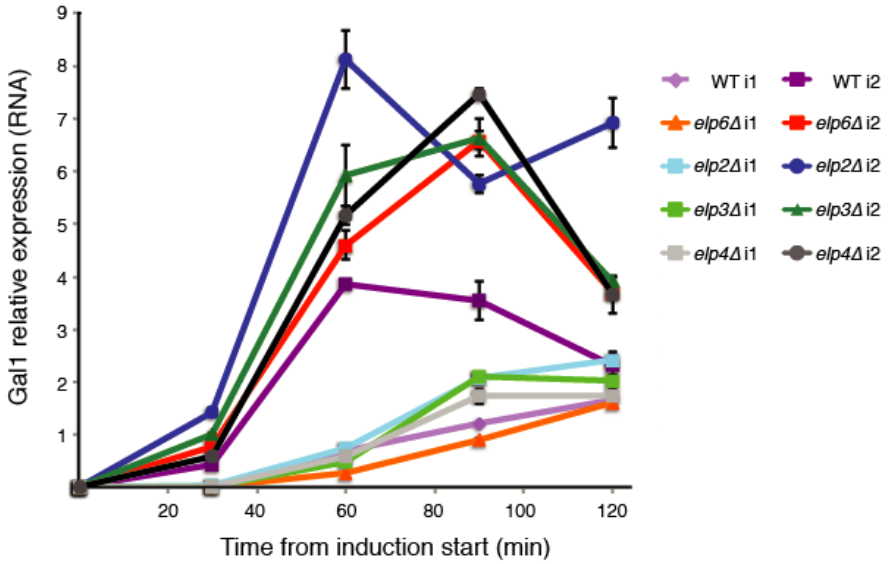

Figure S7. Deletion of individual Elp complex members results in gain-of-memory.

RT-qPCR analysis from strains with deletions of non-essential Elp complex members. The *elp6Δ* gain-of-memory phenotype is representative of other complex members. Error bars calculated as SD from 2 technical replicates, shown is a representative experiment from 2 biological replicates.

Figure S8.

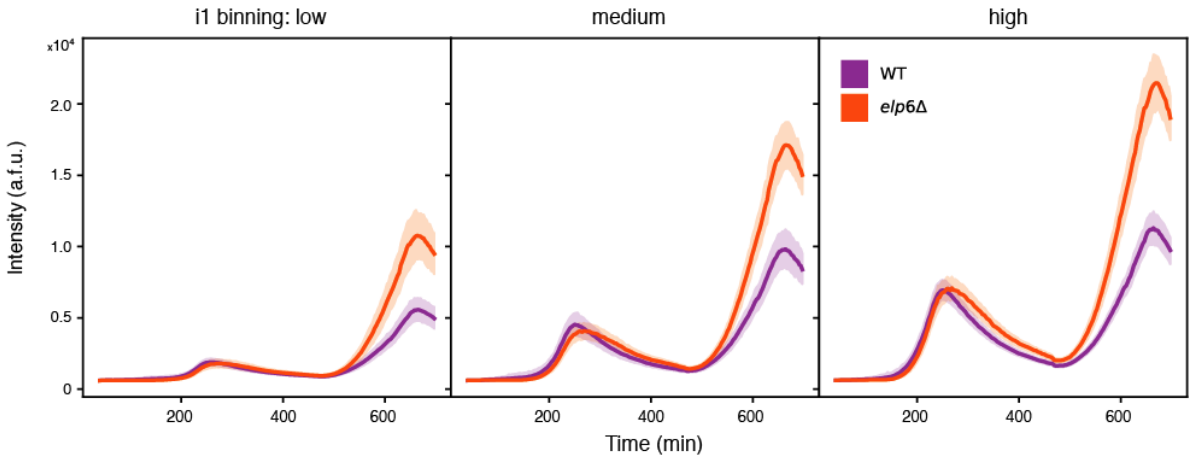

Figure S8. Higher induction in i1 leads to stronger *elp6Δ* gain-of-memory in i2.

WT and *elp6Δ* cells were binned into equivalent low (left), medium (middle), or high (right) i1 expression bins to compare the effect of increasing i1 expression on the gain-of-memory phenotype in *elp6Δ*. Shown is average Gal1-GFP expression (solid line) ±95% confidence intervals (shaded area).

Table S1. Yeast strains.

ID	Name/Description	Genotype	Reference
Y7092	SGA query strain	*MATα; can1Δ::STE2pr-Sp_his5 lyp1Δ his3Δ1 leu2Δ0 ura3Δ0 met15Δ0*	Tong and Boone (2007)
RSY14	Gal1 ORF replaced with GFP, precursor to RSY16	Y7092; *gal1Δ::GFP-kanMX*	This study
RSY15	Precursor to SGA reporter strain RSY17	Y7092; *Gal1-GFP::kanMX*	This study
RSY16	Gal1 ORF replaced with GFP, precursor to RSY19	Y7092; *gal1Δ::GFP-natMX*	This study
RSY17	SGA reporter strain	Y7092; *Gal1-GFP::natMX*	This study
RSY19	Gal1 ORF replaced with GFP, Gal3 tagged with mCherry	Y7092; *gal1Δ::GFP-natMX Gal3-mCherry-His5*	This study
RSY208	WT	RSY17*; Nab2NLS-2mCherry::Ura3*	This study
BY4741	YKO collection parent strain	*MATa; his3Δ1 leu2Δ0 ura3Δ0 met15Δ0*	Brachmann CB, *et al.* (1998)
AK453	SGA WT	*MATa; his3Δ1 leu2Δ0::KanMX ura3Δ0 met15Δ0*	This study
RSY209	*set1Δ*	RSY208; *set1Δ::kanMX*	This study
RSY213	*jhd2Δ*	RSY208; *jhd2Δ::kanMX*	This study
RSY215	*swi2Δ*	RSY208; *swi2Δ::kanMX*	This study
RSY1461	*ach1Δ*	RSY208; *ach1Δ::kanMX*	This study
RSY1462	*bre5Δ*	RSY208; *bre5Δ::kanMX*	This study
RSY1463	*cit1Δ*	RSY208; *cit1Δ::kanMX*	This study
RSY1467	*set3Δ*	RSY208; *set3Δ::kanMX*	This study
RSY1468	*spt2Δ*	RSY208; *spt2Δ::kanMX*	This study
RSY1469	*swc3Δ*	RSY208; *swc3Δ::kanMX*	This study
RSY1470	*ubc4Δ*	RSY208; *ubc4Δ::kanMX*	This study
RSY1471	*hir1Δ*	RSY208; *hir1Δ::kanMX*	This study
RSY1474	*elp6Δ*	RSY208; *elp6Δ::kanMX*	This study
RSY1475	*hos4Δ*	RSY208; *hos4Δ::kanMX*	This study
RSY1480	*rrd1Δ*	RSY208; *rrd1Δ::kanMX*	This study
RSY1481	*sap30Δ*	RSY208; *sap30Δ::kanMX*	This study
RSY1482	*rad61Δ*	RSY208; *rad61Δ::kanMX*	This study
RSY1484	*sub1Δ*	RSY208; *sub1Δ::kanMX*	This study
RSY1485	*uba3Δ*	RSY208; *uba3Δ::kanMX*	This study
RSY1486	*ufd2Δ*	RSY208; *ufd2Δ::kanMX*	This study
RSY1487	*fkh2Δ*	RSY208; *fkh2Δ::kanMX*	This study
RSY1488	*hmt1Δ*	RSY208; *hmt1Δ::kanMX*	This study
RSY1490	*ahc1Δ*	RSY208; *ahc1Δ::kanMX*	This study
RSY1492	*ioc3Δ*	RSY208; *ioc3Δ::kanMX*	This study
RSY1493	*isw2Δ*	RSY208; *isw2Δ::kanMX*	This study
RSY1494	*sas5Δ*	RSY208; *sas5Δ::kanMX*	This study
RSY1496	*sgf29Δ*	RSY208; *sgf29Δ::kanMX*	This study
RSY1497	*spt21Δ*	RSY208; *spt21Δ::kanMX*	This study
RSY1499	*uga3Δ*	RSY208; *uga3Δ::kanMX*	This study
RSY1500	*itc1Δ*	RSY208; *itc1Δ::kanMX*	This study
RSY1522	*elp2Δ*	RSY208; *elp2Δ::kanMX*	This study
RSY1523	*elp3Δ*	RSY208; *elp3Δ::kanMX*	This study
RSY1524	*elp4Δ*	RSY208; *elp4Δ::kanMX*	This study

Table S2. Oligonucleotides.

ID	Name	Sequence 5' to 3'	Function
OL2078	Gal1ORF-sfGFP (f)	GCAGCTGTCTATATGAATTAATGTCCAAGGGTGAAGAGC	to generate PCR product used to transform Y7092 to make RSY15, C-terminal fusion of superfolderGFP to GAL1 with the kanMX marker PCR from plasmid pMaM4
OL2079	TEFt-Gal1downstream (r)	AACAAAGTAAAAAAAAGAAGTATACCAGTATAGCGACCAGCATTC	to generate PCR product used to transform Y7092 to make RSY15, C-terminal fusion of superfolderGFP to GAL1 with the kanMX marker PCR from plasmid pMaM4, and subsequently to replace KanMX marker in RSY15 with the NatMX marker to make RSY17
OL2080	TEFp-natMX (f)	CACATCACATCCGAACATAAACAACCATGACCACTCTTGACGACAC	to replace KanMX marker in RSY15 with the NatMX marker to make RSY17
OL2081	Gal1 271 bp upstream (f)	GCCCCACAAACCTTCAAAT	genotyping of superfolder GFP insertion as a fusion to GAL1
OL2082	sfGFP_A (r)	TTCTCTCTTGCACGTAGCCTT	genotyping of superfolder GFP insertion as a fusion to GAL1
OL2083	Gal1_A (f)	TGGATCATATGGTTCCCGTT	genotyping of superfolder GFP insertion as a fusion to GAL1
OL2084	Gal1_B (r)	AAACGCAGCGGTTGAAAGCAT	genotyping of superfolder GFP insertion as a fusion to GAL1
OL2085	kanB	CTGCAGCGAGGAGCCGTAAT	genotyping KanMX replacements
OL2086	kanC	TGATTTTGATGACGAGCGTAAT	genotyping KanMX replacements
OL2087	natB	TAAGCCGTGTCGTCAAGA	genotyping NatMX replacements
OL2088	natC	TCTGGCTGGAGGTCACCAA	genotyping NatMX replacements
OL2089	PfoI Ura3pr 1110 bp up (f)	CGATAGTCCCGGATTGACAAATGAGAACTTCATGTGGG	to clone in ~1kb Ura3 promoter to create plasmid PL1603 for homology at Ura3 locus in RSY17
OL2090	NdeI Ura3 pr 88 bp up (r)	ACACCACATATGCGTATATATACCAATCTAAGTCTGTGC	to clone in ~1kb Ura3 promoter to create Plasmid PL1603 for homology at Ura3 locus in RSY17
OL2091	Gal1 RT-qPCR (f)	ACACCCTGGAACGGCGATATTGAA	Gal1 RT-qPCR primer
OL2092	Gal1 RT-qPCR(r)	TGAGACTCGTTCATCAAGGCACCA	Gal1 RT-qPCR primer
OL2093	Tcm1 (f)	ACCTCCATTAACCACAAGATTTACA	Tcm1/Rpl3 qPCR primer
OL2094	Tcm1 (r)	AGTCGTTCTTAATTTCACCGTAGTG	Tcm1/Rpl3 qPCR primer
OL2095	*leu2Δ* F	ATATTATAGCTTCTAACGACAATGGAATTCTAACAATTATCAAATTGTCCGCCAGTACATGGAGGCCCAGAATACCCT	to generate PCR fragment to insert KanMX at the Leu2 locus in BY4741 to construct a control strain for SGA
OL2096	*leu2Δ* R	AATCCTCCAATATATAAATTAGGAATCATAGTTTCATGATTTTCTGTTACACCTAACAGTATAGCGACCAGCATTCAC	to generate PCR fragment to insert KanMX at the Leu2 locus in BY4741 to construct a control strain for SGA
OL2097	*leu2Δ* (Fcheck)	CATCAAAATCCACGTTCTTTTCATATGGATTCCT	genotyping KanMX insertion at Leu2 locus
OL2098	*leu2Δ* (Rcheck)	AAACTCCATCAAATGGTCAGGTCATTGAGTGTTT	genotyping KanMX insertion at Leu2 locus
OL2099	*set1Δ::KanMX* (f)	TATTTGTTGAATCTTTATAAGAGGTCTCTGCGTTTAGAGAACATGGAGGCCCAGAATACCC	replacing set1 with KanMX in RSY208
OL2100	*set1Δ::KanMX* (r)	TGTTAAATCAGGAAGCTCCAAACAAATCAATGTATCATCGCAGTATAGCGACCAGCATTCA	replacing set1 with KanMX in RSY208
OL2101	Set1 395 bp upstream (f)	GTTTTGGCCAATTTTATTTACTG	genotyping of *set1Δ::KanMX*
OL2102	Set1 378 bp downstream (r)	TTTTGGTTGAGCGGTATCAG	genotyping of *set1Δ::KanMX*
OL2103	*jhd2Δ::KanMX* (f)	ATTAACTAATCTCATCTTGCACAAAAAACGTATCACTATCACATGGAGGCCCAGAATACCC	replacing jhd2 with KanMX in RSY208
OL2104	*jhd2Δ::KanMX* (r)	TATTCTAAAAAATCATTACGCCATACACAAATATTGAAGACAGTATAGCGACCAGCATTCA	replacing jhd2 with KanMX in RSY208
OL2105	Jhd2 392 bp upstream (f)	ATCCGTATGCTCATCTCGTGA	genotyping of *jhd2Δ::KanMX*
OL2106	Jhd2 390 bp downstream (r)	GCGAAAAGACCCAATTGACCA	genotyping of *jhd2Δ::KanMX*
OL2107	*hir1Δ::KanMX* (f)	AGCATAATAAAATTGCCAGTAACCAAAGGTCTCTGATAACACATGGAGGCCCAGAATACCC	replacing hir1 with KanMX in RSY208
OL2108	*hir1Δ::KanMX* (r)	TGAGGGAAAAAACTTGTCCAAAGGAAGGGGTATAAGCTTACAGTATAGCGACCAGCATTCA	replacing hir1 with KanMX in RSY208
OL2109	Hir1 283 bp upstream (f)	CCCCACAAACTGAAAGCACAT	genotyping of *hir1Δ::KanMX*
OL2110	Hir1 376 bp downstream (r)	CGTGAAAATGGCAAATTTCTC	genotyping of *hir1Δ::KanMX*
OL2111	*swi2Δ::KanMX* (f)	ACTTTCTGCTATTTTCACGACTTTCGATTAATTATCTGCCACATGGAGGCCCAGAATACCC	replacing swi2 with KanMX in RSY208
OL2112	*swi2Δ::KanMX* (r)	CGTATAAACGAATAAGTACTTATATTGCTTTAGGAAGGTACAGTATAGCGACCAGCATTCA	replacing swi2 with KanMX in RSY208
OL2113	Swi2 295 bp upstream (f)	AGGAAAAATAGCCGCCGGTAAA	genotyping of *swi2Δ::KanMX*
OL2114	Swi2 291 bp downstream (r)	GGTCCAAGAACAAGTTCACTATG	genotyping of *swi2Δ::KanMX*
OL2115	*ach1Δ::KanMX* (f)	CAACACATTTCTTTTTTTCTTTTTCACATATTGCACTAAAACATGGAGGCCCAGAATACCC	replacing ach1 with KanMX in RSY208
OL2116	*ach1Δ::KanMX* (r)	TTTTTTGTTAAATACTCATCTCTCGGTTTGCGCACAAACACAGTATAGCGACCAGCATTCA	replacing ach1 with KanMX in RSY208
OL2117	Ach1 289 bp upstream (f)	ACAACGCCCTCAACCACAT	genotyping of *ach1Δ::KanMX*
OL2118	Ach1 298 bp downstream (r)	CGTCATCAGCGAAATTCGTT	genotyping of *ach1Δ::KanMX*
OL2119	*bre5Δ::KanMX* (f)	TGAAGTCATACCCTCGAATAGAAGTATCAAATAAAAGAAAACATGGAGGCCCAGAATACCC	replacing bre5 with KanMX in RSY208
OL2120	*bre5Δ::KanMX* (r)	TTATTTTTTCAATTTTTCTTTTTAAAAGGCTTGTGGTTGACAGTATAGCGACCAGCATTCA	replacing bre5 with KanMX in RSY208
OL2121	Bre5 359 bp upstream (f)	TCACCTACCACAAGCTTTCGT	genotyping of *bre5Δ::KanMX*
OL2122	Bre5 320 bp downstream (r)	TCAAGCTTGCTATCCCCTTC	genotyping of *bre5Δ::KanMX*
OL2123	*cit1Δ::KanMX* (f)	ATAAGGCAAAACATATAGCAATATAATACTATTTACGAAGACATGGAGGCCCAGAATACCC	replacing cit1 with KanMX in RSY208
OL2124	*cit1Δ::KanMX* (r)	TTGAATAGTCGCATACCCTGAATCAAAAATCAAATTTTCCCAGTATAGCGACCAGCATTCA	replacing cit1 with KanMX in RSY208
OL2125	Cit1 299 bp upstream (f)	TGTGTTATTGGAGGATCGCA	genotyping of *cit1Δ::KanMX*
OL2126	Cit1 268 bp downstream (r)	TTACTGCTAAATCAGCGCGCC	genotyping of *cit1Δ::KanMX*
OL2131	*set3Δ::KanMX* (f)	CAGTTTTAGATCGTACTTCACAAAATACGAGAACTGAATCACATGGAGGCCCAGAATACCC	replacing set3 with KanMX in RSY208
OL2132	*set3Δ::KanMX* (r)	TACTTAAGTTTATATAGGTGTAAGAAGGAAATGTCCATGTCAGTATAGCGACCAGCATTCA	replacing set3 with KanMX in RSY208
OL2133	Set3 394 bp upstream (f)	TTCTTTCTGGCTTTTTGCAGT	genotyping of *set3Δ::KanMX*
OL2134	Set3 397 bp downstream (r)	CGCATTGGATAATAATGGCG	genotyping of *set3Δ::KanMX*
OL2135	*spt2Δ::KanMX* (f)	ACAGGGACTTGAGTCCTATTCAAAGTGAAATATTTTAGTTACATGGAGGCCCAGAATACCC	replacing spt2 with KanMX in RSY208
OL2136	*spt2Δ::KanMX* (r)	TCATTTCACGTCCATATATCAAAACATATATCAATATTCCCAGTATAGCGACCAGCATTCA	replacing spt2 with KanMX in RSY208
OL2137	Spt2 378 bp upstream (f)	TGTTGACAAAGCGGAGGAAAG	genotyping of *spt2Δ::KanMX*
OL2138	Spt2 386 bp downstream (r)	GCCGCGAATCTTGTTGAAAA	genotyping of *spt2Δ::KanMX*
OL2139	*swc3Δ::KanMX* (f):	CATGCGATTTGGAAGTAACGCTCGCCGTAGACAAGTAAGAACATGGAGGCCCAGAATACCC	replacing swc3 with KanMX in RSY208
OL2140	*swc3Δ::KanMX* (r)	ATCATAATGGCGTTAAAGCAGAATAAAGTAACCGAACACCCAGTATAGCGACCAGCATTCA	replacing swc3 with KanMX in RSY208
OL2141	Swc3 282 bp upstream (f)	CGGTATTGAAGACACTGACGA	genotyping of *swc3Δ::KanMX*
OL2142	Swc3 293 bp downstream (r)	GGCAAATGGAGGGGATTTTT	genotyping of *swc3Δ::KanMX*
OL2143	*ubc4Δ::KanMX* (f)	TGACTATAGAGTACATACATAAACAAGCATCCAAAAAAACACATGGAGGCCCAGAATACCC	replacing ubc4 with KanMX in RSY208
OL2144	*ubc4Δ::KanMX* (r)	AAATCTTGCTTCTCTTTTTCAGCTGAGTAAGGACTTCTGTCAGTATAGCGACCAGCATTCA	replacing ubc4 with KanMX in RSY208
OL2145	Ubc4 255 bp upstream (f)	ATGGTCTGCGAGATTTTTCC	genotyping of *ubc4Δ::KanMX*
OL2146	Ubc4 256 bp downstream (r)	AATGTTCATGAATCTCCCCTG	genotyping of *ubc4Δ::KanMX*
OL2151	*elp6Δ::KanMX* (f)	ACCGTCCAGAACCTCCACAAAAATAACTAAATACACATTTACATGGAGGCCCAGAATACCC	replacing elp6 with KanMX in RSY208
OL2152	*elp6Δ::KanMX* (r)	TACGAGAATCAATGTGCCTCGTATATAATCTTATCATTATCAGTATAGCGACCAGCATTCA	replacing elp6 with KanMX in RSY208
OL2153	Elp6 274 bp upstream(f)	TGCTGTTGGAAAATTCCTGC	genotyping of *elp6Δ::KanMX*
OL2154	Elp6 263 bp downstream(r)	TGGATAAAATCTGGTGAACGA	genotyping of *elp6Δ::KanMX*
OL2155	*hos4Δ::KanMX* (f)	TATGTGACAGAGAAGAATTGCTGTAGAGATTCATGACAATACATGGAGGCCCAGAATACCC	replacing hos4 with KanMX in RSY208
OL2156	*hos4Δ::KanMX* (r)	AACTATGTATGAGCATATGCCAACGGACCGATGAATTGTTCAGTATAGCGACCAGCATTCA	replacing hos4 with KanMX in RSY208
OL2157	Hos4 250 bp upstream(f)	AAATCAAGGCTCAGGAAGTGA	genotyping of *hos4Δ::KanMX*
OL2158	Hos4 250 bp downstream(r)	CTTTTTTCGTCTTTTGCACGG	genotyping of *hos4Δ::KanMX*
OL2159	*rrd1Δ::KanMX* (f)	AAAGAACGCACATATGAACAAGCATTAAACGAGCAAAGAAACATGGAGGCCCAGAATACCC	replacing rrd1 with KanMX in RSY208
OL2160	*rrd1Δ::KanMX* (r)	TCATAATGCTTGTCATACACATTTATATGTTTAATTAATACAGTATAGCGACCAGCATTCA	replacing rrd1 with KanMX in RSY208
OL2161	Rrd1 287 bp upstream(f)	CCTTTCCATCTGCTCCGAGT	genotyping of *rrd1Δ::KanMX*
OL2162	Rrd1 224 bp downstream(r)	TGTTGTTGTTGCTGCTTCTG	genotyping of *rrd1Δ::KanMX*
OL2163	*sap30Δ::KanMX* (f)	TAGTTTAGCAAATCGAAGGATAGGTATATACTGAGTAGTAACATGGAGGCCCAGAATACCC	replacing sap30 with KanMX in RSY208

OL2164	*sap30Δ::KanMX* (r)	TTACATAACTTATACACAAAAGGGCTGCCTCATCGTTTGACAGTATAGCGACCAGCATTCA	replacing sap30 with KanMX in RSY208
OL2165	Sap30 238 bp upstream(f)	TGGCAGCATAGCACTGTAATG	genotyping of *sap30Δ::KanMX*
OL2166	Sap30 247 bp downstream(r)	TGTAATGCTTTATGGCGCCT	genotyping of *sap30Δ::KanMX*
OL2167	*rad61Δ::KanMX* (f)	AAACCATCTTCTTACCCTAAAGCATCCTGTTTCTGAAAAAACATGGAGGCCCAGAATACCC	replacing rad61 with KanMX in RSY208
OL2168	*rad61Δ::KanMX* (r)	GGTGAAGATGAAGCCAGGCTATGTTCAATGTATGCTTTCTCAGTATAGCGACCAGCATTCA	replacing rad61 with KanMX in RSY208
OL2169	Rad61 257 bp upstream(f)	TGCTTTCAAGCTGGTCTTCA	genotyping of *rad61Δ::KanMX*
OL2170	Rad61 202 bp downstream(r)	AGCGCCATAAGGCATACAAA	genotyping of *rad61Δ::KanMX*
OL2171	*sub1Δ::KanMX* (f)	TACACATCAATTTTTCGACATATATACAAACACAAGCGCTACATGGAGGCCCAGAATACCC	replacing sub1 with KanMX in RSY208
OL2172	*sub1Δ::KanMX* (r)	TGGAAGACGTTGACATAAGCAAGCTCAACTTCCAGGACTACAGTATAGCGACCAGCATTCA	replacing sub1 with KanMX in RSY208
OL2173	Sub1 216 bp upstream(f)	TTTCTCTCTTGGCTTGCCTT	genotyping of *sub1Δ::KanMX*
OL2174	Sub1 239 bp downstream(r)	GTTGTACGGGGAAAATGCTT	genotyping of *sub1Δ::KanMX*
OL2175	*uba3Δ::KanMX* (f)	GATATTGTATACCTATATTATCGATAATAAAGCGACGAGGACATGGAGGCCCAGAATACCC	replacing uba3 with KanMX in RSY208
OL2176	*uba3Δ::KanMX* (r)	AACAAGTGACACCGGCGGATGGTATTATTCATTAGTAATACAGTATAGCGACCAGCATTCA	replacing uba3 with KanMX in RSY208
OL2177	Uba3 350 bp upstream(f)	TTTATGCATTTGGCTCCTGT	genotyping of *uba3Δ::KanMX*
OL2178	Uba3 245 bp downstream(r)	TGTGATCAACGGCTCCTTAGT	genotyping of *uba3Δ::KanMX*
OL2179	*ufd2Δ::KanMX* (f)	AAAAGTTAACTTTGAAAGTAGAACCCTCATTCCATAGATCACATGGAGGCCCAGAATACCC	replacing ufd2 with KanMX in RSY208
OL2180	*ufd2Δ::KanMX* (r)	ATTAGGGTCAATTTTGCAATTTATTCTATCACTTATTCATCAGTATAGCGACCAGCATTCA	replacing ufd2 with KanMX in RSY208
OL2181	Ufd2 226 bp upstream(f)	TTCTAACCATTGGCAACAAAA	genotyping of *ufd2Δ::KanMX*
OL2182	Ufd2 236 bp downstream(r)	AGAAGCAAATCGCTTTCCCA	genotyping of *ufd2Δ::KanMX*
OL2183	*fkh2Δ::KanMX* (f)	CCTCCGTTTCCTTTATTGAAACTTTATCAATGCGCAAGAAACATGGAGGCCCAGAATACCC	replacing fkh2 with KanMX in RSY208
OL2184	*fkh2Δ::KanMX* (r)	TTCATTTCTTTAGTCTTAGTGATTCACCTTGTTTCTTGTCCAGTATAGCGACCAGCATTCA	replacing fkh2 with KanMX in RSY208
OL2185	Fkh2 287 bp upstream (f)	ATGGTTCCGCATTTCTAAAGG	genotyping of *fkh2Δ::KanMX*
OL2186	Fkh2 287 bp downstream(r)	TCAAGGATGCAAACACAGCA	genotyping of *fkh2Δ::KanMX*
OL2187	*hmt1Δ::KanMX* (f)	AAAAAAGAGTTAGAACCGACAAATTCATCCAAAGAAAATAACATGGAGGCCCAGAATACCC	replacing hmt1 with KanMX in RSY208
OL2188	*hmt1Δ::KanMX* (r)	TGCTTTTCAAATTTTTTTCTTTCTCCAGCAAACAAAAGTCCAGTATAGCGACCAGCATTCA	replacing hmt1 with KanMX in RSY208
OL2189	Hmt1 299 bp upstream (f)	CCCATGAGGGACTGTTAATGA	genotyping of *hmt1Δ::KanMX*
OL2190	Hmt1 294 bp downstream(r)	TTGCCGACATAGGTTGGAAA	genotyping of *hmt1Δ::KanMX*
OL2191	*ahc1Δ::KanMX* (f)	CGCTTCTCATCCAACACTTTGTGTATATGTCCATCTCCTCACATGGAGGCCCAGAATACCC	replacing ahc1 with KanMX in RSY208
OL2192	*ahc1Δ::KanMX* (r)	GAATATTATATTACGTAATTTACTTATTTATATGTGTGTACAGTATAGCGACCAGCATTCA	replacing ahc1 with KanMX in RSY208
OL2193	Ahc1 199 bp upstream(f)	AGGAAGAGCAGACAGCAAGAA	genotyping of *ahc1Δ::KanMX*
OL2194	Ahc1 200 bp down(r)	TAAAACGAGTGCTGGAGGGAA	genotyping of *ahc1Δ::KanMX*
OL2199	*ioc3Δ::KanMX* (f)	ACCAAGTACTTCAAGCAAAGTTTGCAATCCCCTATTGTTTACATGGAGGCCCAGAATACCC	replacing ioc3 with KanMX in RSY208
OL2200	*ioc3Δ::KanMX* (r)	AGGAGTTTCACAATCTTCACGTTCGTTGAAAGCTAGTTGTCAGTATAGCGACCAGCATTCA	replacing ioc3 with KanMX in RSY208
OL2201	Ioc3 250 bp upstream(f)	TGGCGGTATTTGTTAACATTG	genotyping of *ioc3Δ::KanMX*
OL2202	Ioc3 240 bp down(r)	CGTTTTACCACACTGGCGAAT	genotyping of *ioc3Δ::KanMX*
OL2203	*isw2Δ::KanMX* (f)	TGGTTTAAGTCGTAACAAAAGGAAAACTTACAATCAGATCACATGGAGGCCCAGAATACCC	replacing isw2Δ with KanMX in RSY208
OL2204	*isw2Δ::KanMX* (r)	ATATCTCTCACGTCACTTATTTTAATGCACAATACATGATCAGTATAGCGACCAGCATTCA	replacing isw2Δ with KanMX in RSY208
OL2205	Isw2 229 bp upstream(f)	CGTAACGTACGTACAATGGCT	genotyping of *isw2Δ::KanMX*
OL2206	Isw2 229 bp down(r)	CATTCACCATTTTTGCAGCG	genotyping of *isw2Δ::KanMX*
OL2207	*sas5Δ::KanMX* (f)	CTTTTTTTTTTTTTGGTGCCATATAATAGACGCTCTTTTACATGGAGGCCCAGAATACCC	replacing sas5 with KanMX in RSY208
OL2208	*sas5Δ::KanMX* (r)	CTATGTTTTCAGGCATTGTTTAATTTCATGATGGCTGTCCCAGTATAGCGACCAGCATTCA	replacing sas5 with KanMX in RSY208
OL2209	Sas5 229 bp upstream(f)	TTAGTGACGTTTACAGCTGGC	genotyping of *sas5Δ::KanMX*
OL2210	Sas5 246 bp down(r)	GTTCTGTGGAAGCGCAAAAA	genotyping of *sas5Δ::KanMX*
OL2215	*sgf29Δ::KanMX* (f)	GGAGTTTTTCACAGCAAAACACACGGTCACCTTTCTTATTACATGGAGGCCCAGAATACCC	replacing sgf29 with KanMX in RSY208
OL2216	*sgf29Δ::KanMX* (r)	AGAAGATCTTATGATATGTAGTAAATGTTAACCACCATTGCAGTATAGCGACCAGCATTCA	replacing sgf29 with KanMX in RSY208
OL2217	Sgf29 244 bp upstream(f)	CCCTCGGGACTCTCCTCTATA	genotyping of *sgf29Δ::KanMX*
OL2218	Sgf29 220 bp down(r)	CTCTCCATCTTGGCGAAAAA	genotyping of *sgf29Δ::KanMX*
OL2219	*spt21Δ::KanMX* (f)	ATTGGAATTGGTATTCACTTGAACAAAAGACTCTGGTAAAACATGGAGGCCCAGAATACCC	replacing spt21 with KanMX in RSY208
OL2220	*spt21Δ::KanMX* (r)	TATATACATGCTGTGCTAGGAATAAGTTCATGTAATATTTCAGTATAGCGACCAGCATTCA	replacing spt21 with KanMX in RSY208
OL2221	Spt21 236 bp upstream(f)	AAACGCGTCGCGTTAGAAAA	genotyping of *spt21Δ::KanMX*
OL2222	Spt21 235 bp down(r)	TCAAGGAGACAATTTCCGCT	genotyping of *spt21Δ::KanMX*
OL2223	*uga3Δ::KanMX* (f)	TGTATGGATGCCAAGAAAACAAAGTTTTTTAAAGTGAGGTACATGGAGGCCCAGAATACCC	replacing uga3 with KanMX in RSY208
OL2224	*uga3Δ::KanMX* (r)	TTAAGACACCCAGGGGGCGGGGAAAGAAAATATATGCTGCCAGTATAGCGACCAGCATTCA	replacing uga3 with KanMX in RSY208
OL2225	Uga3 249 bp upstream(f)	CATCACGTTCGTCGTGACATA	genotyping of *uga3Δ::KanMX*
OL2226	Uga3 247 bp down(r)	TTACAGGTATCAAACCGGGCA	genotyping of *uga3Δ::KanMX*
OL2227	*itc1Δ::KanMX* (f)_2	AAAAAAAGAAAATAACAATAGGAGGAAGTAAAGAAAGCCGTTAATAAACAACATGGAGGCCCAGAATACCC	replacing itc1 with KanMX in RSY208
OL2228	*itc1Δ::KanMX* (r)_2	TTTATGAATACTACAATTTACCATCAGTTACAAAGGAAGTTTTTTATATACAGTATAGCGACCAGCATTCA	replacing itc1 with KanMX in RSY208
OL2229	Itc1 358 bp upstream (f)	TTAACGTGGTGAGAAAACCCG	genotyping of *itc1Δ::KanMX*
OL2230	Itc1 389 bp downstream (r)	TGCCCACATTGTGGTACAAA	genotyping of *itc1Δ::KanMX*
OL2231	*elp2Δ::KanMX* (f)	AGTTCCTGCAAAAACTTTATATAGTTAACGTTCCATAATCACATGGAGGCCCAGAATACCC	replacing elp2 with KanMX in RSY208
OL2232	*elp2Δ::KanMX* (r)	TATCCTCTTCTTTTCACATGAGAAATGATATAGATATTGCCAGTATAGCGACCAGCATTCA	replacing elp2 with KanMX in RSY208
OL2233	Elp2 276 bp upstream (f)	GAGACTGAGATGCAACCCATT	genotyping of *elp2Δ::KanMX*
OL2234	Elp2 280 bp down (r)	GAGTCCATTGGATGGTCAAA	genotyping of *elp2Δ::KanMX*
OL2235	*elp3Δ::KanMX* (f)	TAAAAGCACCTAAGGAAAATCGAAGAACACCCTGACAAAGACATGGAGGCCCAGAATACCC	replacing elp3 with KanMX in RSY208
OL2236	*elp3Δ::KanMX* (r)	AACCGGCCATGTCGGCGGCACATAAAAGTTCTATTTACCTCAGTATAGCGACCAGCATTCA	replacing elp3 with KanMX in RSY208
OL2237	Elp3 190 bp upstream (f)	TCTGCCGCTTTCATTGTTT	genotyping of *elp3Δ::KanMX*
OL2238	Elp3 225 bp down (r)	TTCGTTCCTTCCCTTCTGTT	genotyping of *elp3Δ::KanMX*
OL2239	*elp4Δ::KanMX* (f)	CATTGTATAACAAATTCGGCTCCCAAATATCGCATGTACCACATGGAGGCCCAGAATACCC	replacing elp4 with KanMX in RSY208
OL2240	*elp4Δ::KanMX* (r)	AAAAGCATGCCGTATATTTCCCATAAATTGAACCATATTCCAGTATAGCGACCAGCATTCA	replacing elp4 with KanMX in RSY208
OL2241	Elp4 282 bp upstream (f)	TTGCACAAGCATTTTGCTGG	genotyping of *elp4Δ::KanMX*
OL2242	Elp4 271 bp down (r)	TCAAATCCAAAGGAGTGGAA	genotyping of *elp4Δ::KanMX*
OL2243	Gal1 ChIP (f)	GGAAAAGCTGCATAACCACTTTAAC	Gal1 promoter ChIP-qPCR primer
OL2244	Gal1 ChIP (r)	CAATCACTTCTTCTGAATGAGATTT	Gal1 promoter ChIP-qPCR primer
OL2282	Gal1MN1401 (f)	AAATTAACGAATCAAATTAACAACCATAG	Gal1 promoter MNase-qPCR primer
OL2283	Gal1MN1401 (r)	CCAGAAATAAGGCTAAAAAACTAATC	Gal1 promoter MNase-qPCR primer
OL2306	Gal1promoter-sfGFP (f)	TTAACGTCAAGGAGAAAAAACTATAATGTCCAAGGGTGAAGAGC	to generate PCR product used to transform Y7092 to make RSY14, replacement of GAL1 with superfolderGFP and the kanMX marker PCR from plasmid pMaM4
OL2307	Gal3ORF-mCherry (f)	AGTTTCGAAGCCTGCCTTGGGTACTTGTTTGTACGAACAAATGGTGAGCAAGGGCGAGGA	to generate PCR product used to transform Y16 to make RSY19, replacement of GAL1 with superfolderGFP and a C-terminal fusion of mCherry to GAL3 with the His5 marker PCR from plasmid pKT355
OL2308	Gal3ORF-mCherry (r)	CTTTTAATATTTAAAGGTTGTTCCAAGAAGGTGTTTAGTGTTACAACACTCCCTTCGTGC	to generate PCR product used to transform Y16 to make RSY19, replacement of GAL1 with superfolderGFP and a C-terminal fusion of mCherry to GAL3 with the His5 marker PCR from plasmid pKT355

Table S3. Statistical tests and exact *P*-values

Figure	Comparison	Statistical test	paired	one-sided or two-sided	Multiple testing correction	*P*-value	test statistic
1D, left	WT M1 vs. M2 intensity	Mann-Whitney U	yes	two	none	1.7E-27	8.0E+02
1D, middle	WT M1 vs. M2 delay	Mann-Whitney U	yes	two	none	3.5E-28	0.0E+00
1D, right	WT M1 vs. M2 expression rate	Mann-Whitney U	yes	two	none	1.2E-01	4.7E+03
2B	D2 vs. M1	Kolmogorov-Smirnov	no	two	none	1.5E-48	7.8E-01
2B	D2 vs. M2	Kolmogorov-Smirnov	no	two	none	1.6E-01	1.1E-01
2C	M2-D2 vs. U M2-D2	Mann-Whitney U	no	two	none	7.8E-30	1.7E+04
2D	1 vs. 1+2+3	Mann-Whitney U	no	two	none	3.7E-01	2.9E+03
2D	2 vs. 1+2+3	Mann-Whitney U	no	two	none	9.4E-01	5.6E+03
2D	3 vs. 1+2+3	Mann-Whitney U	no	two	none	3.3E-01	2.5E+03
2E	WT raf+CHX vs. gal/raf+CHX	Kolmogorov-Smirnov	no	two	none	2.1E-27	5.6E-01
3D	*cit1Δ* vs. WT	Anderson-Darling	no	two	none	9.1E-06	1.8E+01
3D	*set3Δ* vs. WT	Anderson-Darling	no	two	none	1.0E-05	2.4E+01
3D	*elp6Δ* vs. WT	Anderson-Darling	no	two	none	7.5E-04	7.2E+00
4A	*cit1Δ* vs. WT	Mann-Whitney U	no	two	Bonferroni	6.6E-06	1.6E+04
4A	*set3Δ* vs. WT	Mann-Whitney U	no	two	Bonferroni	3.0E-01	5.3E+03
4A	*elp6Δ* vs. WT	Mann-Whitney U	no	two	Bonferroni	7.6E-04	7.3E+03
4B, left	*cit1Δ* vs. WT	Mann-Whitney U	no	two	Bonferroni	1.1E-08	1.7E+04
4B, left	*set3Δ* vs. WT	Mann-Whitney U	no	two	Bonferroni	4.5E-02	5.6E+03
4B, left	*elp6Δ* vs. WT	Mann-Whitney U	no	two	Bonferroni	2.0E-01	1.1E+04
4B, right	*cit1Δ* vs. WT	Mann-Whitney U	no	two	Bonferroni	2.0E-10	1.8E+04
4B, right	*set3Δ* vs. WT	Mann-Whitney U	no	two	Bonferroni	2.4E-02	5.7E+03
4B, right	*elp6Δ* vs. WT	Mann-Whitney U	no	two	Bonferroni	2.8E-02	8.0E+03
4D	*cit1Δ* vs. WT	Mann-Whitney U	no	two	Bonferroni	1.2E-04	4.5E+04
4D	*set3Δ* vs. WT	Mann-Whitney U	no	two	Bonferroni	7.4E-01	2.2E+04
4D	*elp6Δ* vs. WT	Mann-Whitney U	no	two	Bonferroni	2.0E+00	3.8E+04
4E	*cit1Δ* vs. WT	Mann-Whitney U	no	two	Bonferroni	4.7E-02	5.0E+04
4E	*set3Δ* vs. WT	Mann-Whitney U	no	two	Bonferroni	1.0E+00	1.0E+04
4E	*elp6Δ* vs. WT	Mann-Whitney U	no	two	Bonferroni	2.9E-02	3.8E+04
5E	*cit1Δ* vs. WT in r1	t-test	no	two	Bonferroni	2.6E-01	
5E	*set3Δ* vs. WT in r1	t-test	no	two	Bonferroni	1.9E-01	
5E	*elp6Δ* vs. WT in r1	t-test	no	two	Bonferroni	5.7E-01	
5E	*cit1Δ* vs. WT in r2	t-test	no	two	Bonferroni	7.2E-02	
5E	*set3Δ* vs. WT in r2	t-test	no	two	Bonferroni	2.3E-01	
5E	*elp6Δ* vs. WT in r2	t-test	no	two	Bonferroni	5.1E-04	

Table S4. Gene list of deletion mutants used for library construction

Systematic name	Standard name	Systematic name	Standard name	Systematic name	Standard name	Systematic name	Standard name	Systematic name	Standard name	Systematic name	Standard name
YAL011W	SWC3	YDL059C	RAD59	YER116C	SLX8	YIL110W	HPM1	YLR306W	UBC12	YNL330C	RPD3
YAL013W	DEP1	YDL070W	BDF2	YER123W	YCK3	YIL112W	HOS4	YLR307W	CDA1	YNR001C	CIT1
YAL017W	PSK1	YDL074C	BRE1	YER142C	MAG1	YIL122W	POG1	YLR308W	CDA2	YNR010W	CSE2
YAL019W	FUN30	YDL076C	RXT3	YER144C	UBP5	YIL128W	MET18	YLR320W	MMS22	YNR024W	HXT17
YAL029C	MYO4	YDL090C	RAM1	YER151C	UBP3	YIL131C	FKH1	YLR335W	NUP2	YNR051C	BRE5
YAL036C	RBG1	YDL102W	STE20	YER161C	SPT2	YIL153W	RRD1	YLR377C	GAL80	YNR072W	RTS2
YAL049C	AIM2	YDL112W	TRM3	YER162C	RAD4	YIL156W	UBP7	YLR381W	CTF3	YOL001W	PHO80
YAL051W	OAF1	YDL115C	NVJ1	YER164W	CHD1	YIL160C	POT1	YLR384C	IKI3	YOL004W	SIN3
YAL054C	ACS1	YDL122W	UBP1	YER167W	BCK2	YIL162W	MIG1	YLR385C	SWC7	YOL006C	TOP1
YAR002W	NUP60	YDL131W	LYS21	YER177W	BMH1	YIR001C	SNT2	YLR394W	CST9	YOL012C	HTZ1
YAR003W	SWD1	YDL134C	PPH21	YER178W	PDA1	YIR002C	MPH1	YLR418C	CDC73	YOL017W	ESC8
YAR015W	ADE1	YDL160C-A	SUC2	YER179W	DMC1	YIR005W	IST3	YLR421C	RPN13	YOL054W	PSH1
YAR020C	PAU7	YDL170W	UGA3	YFL001W	DEG1	YIR009W	MSL1	YLR449W	FPR4	YOL067C	RTG1
YAR050W	FLO1	YDL175C	AIR2	YFL007W	BLM3	YIR023W	DAL81	YLR453C	RIF2	YOL068C	HST1
YBL001C	ECM15	YDL182W	LYS20	YFL013C	IES1	YIR025W	MND2	YML005W	TRM12	YOL086W-A	PIP2
YBL003C	HTA2	YDL185W	TFP1	YFL023W	BUD27	YJL030W	MAD2	YML028W	TSA1	YOL090W	MSH2
YBL008W	HIR1	YDL188C	PPH22	YFL049W	SWP82	YJL047C	RTT101	YML032C	RAD52	YOL104C	NDJ1
YBL015W	ACH1	YDL190C	UFD2	YFR010W	UBP6	YJL065C	DLS1	YML034W	SRC1	YOL108C	INO4
YBL016W	FUS3	YDL194W	SNF3	YFR013W	IOC3	YJL092W	HPR5	YML041C	VPS71	YOR001W	RRP6
YBL031W	SHE1	YDL213C	NOP6	YFR034C	PHO4	YJL105W	SET4	YML042W	CAT2	YOR005C	DNL4
YBL037W	APL3	YDL224C	WHI4	YFR038W	IRC5	YJL115W	ASF1	YML051W	ERG13	YOR014W	RTS1
YBL046W	PSY4	YDL227C	HO	YGL004C	RPN14	YJL124C	LSM1	YML060W	OGG1	YOR021C	SFM1
YBL052C	SAS3	YDR004W	RAD57	YGL019W	CKB1	YJL148W	RPA34	YML062C	MFT1	YOR023C	AHC1
YBL054W	TOD6	YDR009W	SGN1	YGL035C	MSN4	YJL168C	SET2	YML074C	FPR3	YOR025W	HST3
YBL067C	UBP13	YDR014W	RAD61	YGL043W	DST1	YJL173C	MPT5	YML094W	GIM5	YOR033C	EXO1
YBL088C	TEL1	YDR059C	UBC5	YGL058W	RAD6	YJL176C	SWI3	YML095C	RAD10	YOR038C	HIR2
YBL089W	AVT5	YDR073W	SNF11	YGL060W	YBP2	YJL187C	SWE1	YML102W	CAC2	YOR039W	CKB2
YBL091C-A	SCS22	YDR075W	PPH3	YGL066W	SGF73	YJL197W	UBP12	YML109W	ZDS2	YOR061W	CKA2
YBL103C	RTG3	YDR076W	RAD55	YGL087C	MMS2	YJR021C	REC107	YML111W	BUL2	YOR064C	YNG1
YBR005W	RCR1	YDR083W	RRP8	YGL090W	LIF1	YJR032W	CPR7	YML121W	GTR1	YOR077W	ERG10
YBR006W	UGA2	YDR092W	UBC13	YGL096W	TOS8	YJR035W	RAD26	YML126C	MSN2	YOR100C	CRC1
YBR007C	DSF2	YDR096W	GIS1	YGL115W	SNF4	YJR036C	HUL4	YMR021C	MAC1	YOR123C	LEO1
YBR009C	HHF1	YDR097C	MSH6	YGL127C	SOH1	YJR043C	POL32	YMR022W	QRI8	YOR124C	UBP2
YBR010W	HHT1	YDR121W	DPB4	YGL131C	RSM22	YJR052W	RAD7	YMR036C	MIH1	YOR144C	ELG1
YBR014C	GRX7	YDR139C	RUB1	YGL133W	ITC1	YJR082C	EAF6	YMR037C	NAM7	YOR156C	NFI1
YBR030W	RKM3	YDR143C	SAN1	YGL136C	MRM2	YJR090C	RFA3	YMR039C	SUB1	YOR162C	YRR1
YBR031W	RPL4a	YDR146C	SWI5	YGL151W	NUT1	YJR099W	YUH1	YMR044W	IOC4	YOR172W	YRM1
YBR034C	HMT1	YDR155C	CPR1	YGL163C	RAD54	YJR119C	JHD2	YMR048W	CSM3	YOR189W	IES4
YBR046C	ZTA1	YDR156W	RPA14	YGL168W	HUR1	YJR135C	MCM22	YMR075W	RCO1	YOR191W	RIS1
YBR057C	MUM2	YDR159W	SAC3	YGL173C	KEM1	YJR140C	HIR3	YMR078C	CTF18	YOR195W	SLK19
YBR058C	UBP14	YDR174W	HMO1	YGL174W	BUD13	YKL010C	UFD4	YMR080C	MPP6	YOR202W	HIS3
YBR061C	TRM7	YDR181C	SAS4	YGL175C	SAE2	YKL020C	SPT23	YMR100W	MUB1	YOR213C	SAS5
YBR072W	HSP26	YDR191W	HST4	YGL178W	POL3	YKL023W	SKA1	YMR106C	YKU80	YOR239W	ABP140
YBR073W	RDH54	YDR198C	RKM2	YGL194C	HOS2	YKL033W	TTI1	YMR127C	SAS2	YOR279C	RFM1
YBR082C	UBC4	YDR207C	UME6	YGL213C	SKI8	YKL062W	GRR1	YMR133W	REC114	YOR304W	ISW2
YBR083W	TEC1	YDR214W	AHA1	YGL222C	EDC1	YKL101W	HSL1	YMR135C	GID8	YOR308C	SNU66
YBR094W	PBY1	YDR217C	RAD9	YGL227W	VID30	YKL110C	KTI12	YMR138W	CIN4	YOR338W	YOR338W
YBR095C	RXT2	YDR225W	HTA1	YGL244W	RTF1	YKL113C	RAD27	YMR167W	MLH1	YOR339C	UBC11
YBR098W	MMS4	YDR254W	CHL4	YGL249W	ZIP2	YKL117W	SBA1	YMR176W	ECM5	YOR346W	REV1
YBR103W	SIF2	YDR255C	RMD5	YGL252C	RTG2	YKL149C	DBR1	YMR179W	SPT21	YOR349W	CIN1
YBR107C	IML3	YDR257C	SET7	YGR078C	PAC10	YKL155C	BRE2	YMR190C	SGS1	YOR351C	MEK1
YBR111C	YSA1	YDR260C	SWM1	YGR086C	PIL1	YKL160W	ELF1	YMR207C	HFA1	YOR363C	MHF1
YBR114W	RAD16	YDR266C	HEL2	YGR097W	ASK10	YKL213C	DOA1	YMR209C	YMR209C	YPL001W	HAT1
YBR119W	MUD1	YDR289C	RTT103	YGR121C	MEP1	YKR010C	TOF2	YMR216C	SKY1	YPL008W	CHL1
YBR141C	BMT2	YDR310C	SUM1	YGR134W	CAF130	YKR017C	HEL1	YMR219W	ESC1	YPL015C	HST2
YBR162W-A	YSY6	YDR316W	OMS1	YGR135W	PRE9	YKR028W	SAP190	YMR223W	UBP8	YPL018W	CTF19
YBR169C	SSE2	YDR318W	MCM21	YGR163W	GTR2	YKR029C	SET3	YMR224C	MRE11	YPL022W	RAD1
YBR175W	SWD3	YDR334W	SWR1	YGR184C	UBR1	YKR048C	NAP1	YMR247C	RKR1	YPL024W	NCE4
YBR194W	SOY1	YDR359C	VID21	YGR188C	BUB1	YKR056W	TRM2	YMR263W	SAP30	YPL028W	MHF2
YBR195C	MSI1	YDR363W	ESC2	YGR200C	ELP2	YKR069W	MET1	YMR272C	SCS7	YPL046C	ELC1
YBR208C	DUR1,2	YDR363W-A	SEM1	YGR208W	SER2	YKR072C	SIS2	YMR273C	ZDS1	YPL047W	SGF11
YBR215W	HPC2	YDR369C	XRS2	YGR212W	SLI1	YKR077W	MSA2	YMR275C	BUL1	YPL055C	LGE1
YBR228W	SLX1	YDR378C	LSM6	YGR270W	YTA7	YKR082W	NUP133	YMR284W	YKU70	YPL086C	ELP3
YBR231C	SWC5	YDR386W	MUS81	YGR275W	RTT102	YKR098C	UBP11	YMR304W	UBP15	YPL101W	ELP4
YBR245C	ISW1	YDR392W	SPT3	YHL007C	IWR1	YKR101W	SIR1	YMR312W	ELP6	YPL116W	HOS3
YBR258C	SHG1	YDR409W	SIZ1	YHL022C	SPO11	YLL002W	RTT109	YNL004W	HRB1	YPL127C	HHO1
YBR261C	TAE1	YDR419W	RAD30	YHL039W	EFM1	YLL039C	UBI4	YNL021W	HDA1	YPL138C	SPP1
YBR271W	EFM2	YDR423C	CAD1	YHR031C	RRM3	YLL062C	MHT1	YNL022C	RCM1	YPL139C	UME1
YBR274W	CHK1	YDR435C	PPM1	YHR034C	PIH1	YLR015W	GAL2	YNL030W	HHF2	YPL152W	RRD2
YBR275C	RIF1	YDR440W	DOT1	YHR041C	SRB2	YLR024C	UBR2	YNL031C	HHT2	YPL165C	SET6
YBR278W	DPB3	YDR451C	YHP1	YHR081W	LRP1	YLR032W	RAD5	YNL063W	MTQ1	YPL167C	REV3
YCL010C	SGF29	YDR465C	RMT2	YHR109W	CTM1	YLR039C	RIC1	YNL068C	FKH2	YPL181W	CTI6
YCL011C	GBP2	YDR469W	SDC1	YHR115C	DMA1	YLR044C	PDC1	YNL071W	LAT1	YPL184C	MRN1
YCL016C	DCC1	YDR477W	SNF1	YHR129C	ARP1	YLR055C	SPT8	YNL092W	YNL092W	YPL208W	RKM1
YCL032W	STE50	YDR482C	CWC21	YHR154W	RTT107	YLR056W	ERG3	YNL097C	PHO23	YPL226W	NEW1
YCL037C	SRO9	YDR485C	VPS72	YHR157W	REC104	YLR063W	BMT6	YNL098C	RAS2	YPL248C	GAL4
YCL061C	MRC1	YDR501W	PLM2	YHR167W	THP2	YLR081W	FBP1	YNL107W	YAF9	YPL273W	SAM4
YCR005C	CIT2	YDR519W	FPR2	YHR178W	STB5	YLR085C	ARP6	YNL135C	FPR1	YPR001W	CIT3
YCR028C-A	RIM1	YEL003W	GIM4	YHR191C	CTF8	YLR095C	IOC2	YNL136W	EAF7	YPR007C	REC8
YCR033W	SNT1	YEL012W	UBC8	YHR195W	GAL3	YLR102C	APC9	YNL147W	LSM7	YPR018W	RLF2
YCR060W	TAH1	YEL037C	RAD23	YHR200W	RPN10	YLR135W	SLX4	YNL153C	GIM3	YPR023C	EAF3
YCR065W	HCM1	YEL056W	HAT2	YHR207C	SET5	YLR137W	RKM5	YNL199C	GCR2	YPR031W	NTO1
YCR075C	ERS1	YEL066W	HPA1	YHR209W	CRG1	YLR172C	DPH5	YNL201C	PSY2	YPR046W	MCM16
YCR076C	FUB1	YER007W	PAC2	YIL010W	DOT5	YLR180W	SAM1	YNL206C	RTT106	YPR052C	NHP6A
YCR077C	PAT1	YER027C	GAL83	YIL017C	VID28	YLR182W	SWI6	YNL215W	IES2	YPR066W	UBA3
YCR081W	SRB8	YER030W	CHZ1	YIL035C	CKA1	YLR183C	TOS4	YNL218W	MGS1	YPR068C	HOS1
YCR082W	AHC5	YER035W	EDC2	YIL036W	CST6	YLR200W	YKE2	YNL224C	SQS1	YPR070W	MED1
YCR086W	CSM1	YER051W	JHD1	YIL040W	APQ12	YLR216C	CPR6	YNL246W	VPS75	YPR093C	ASR1
YCR092C	MSH3	YER063W	THO1	YIL064W	SEE1	YLR233C	EST1	YNL253W	TEX1	YPR119W	CLB2
YDL002C	NHP10	YER088C	DOT6	YIL066C	RNR3	YLR234W	TOP3	YNL273W	TOF1	YPR135W	CTF4
YDL013W	HEX3	YER092W	IES5	YIL079C	AIR1	YLR247C	IRC20	YNL288W	CAF40	YPR164W	MMS1
YDL020C	RPN4	YER095W	RAD51	YIL084C	SDS3	YLR263W	RED1	YNL298W	CLA4	YPR179C	HDA3
YDL051W	LHP1	YER098W	UBP9	YIL096C	BMT5	YLR278C	YLR278C	YNL299W	TRF5	YPR193C	HPA2
YDL056W	MBP1	YER111C	SWI4	YIL097W	FYV10	YLR285W	NNT1	YNL307C	MCK1		